Hadron optics in three-dimensional invariant coordinate space from deeply virtual Compton scattering

S. J. Brodsky,[1] D. Chakrabarti,[2] A. Harindranath,[3] A. Mukherjee,[4] and J. P. Vary[1,5,6]

[1]*Stanford Linear Accelerator Center, Stanford University, Stanford, California 94309, USA*
[2]*Department of Physics, University of Florida, Gainesville, Florida-32611-8440, USA*
[3]*Saha Institute of Nuclear Physics, 1/AF Bidhannagar, Kolkata 700064, India*
[4]*Department of Physics, Indian Institute of Technology, Powai, Mumbai 400076, India*
[5]*Department of Physics and Astronomy, Iowa State University, Ames, Iowa 50011, USA*
[6]*Lawrence Livermore National Laboratory, L-414, 7000 East Avenue, Livermore, California, 94551, USA*

(Received 2 November 2006; published 3 January 2007)

The Fourier transform of the deeply virtual Compton scattering amplitude (DVCS) with respect to the skewness parameter $\zeta = Q^2/2p \cdot q$ can be used to provide an image of the target hadron in the boost-invariant variable σ, the coordinate conjugate to light-front time $\tau = t + z/c$. As an illustration, we construct a consistent covariant model of the DVCS amplitude and its associated generalized parton distributions using the quantum fluctuations of a fermion state at one loop in QED, thus providing a representation of the light-front wave functions (LFWFs) of a lepton in σ space. A consistent model for hadronic amplitudes can then be obtained by differentiating the light-front wave functions with respect to the bound-state mass. The resulting DVCS helicity amplitudes are evaluated as a function of σ and the impact parameter $\vec{b}_\perp$, thus providing a light-front image of the target hadron in a frame-independent three-dimensional light-front coordinate space. Models for the LFWFs of hadrons in $(3 + 1)$ dimensions displaying confinement at large distances and conformal symmetry at short distances have been obtained using the AdS/CFT method. We also compute the LFWFs in this model in invariant three-dimensional coordinate space. We find that, in the models studied, the Fourier transform of the DVCS amplitudes exhibit diffraction patterns. The results are analogous to the diffractive scattering of a wave in optics where the distribution in σ measures the physical size of the scattering center in a one-dimensional system.

DOI: 10.1103/PhysRevD.75.014003 PACS numbers: 13.60.Fz, 12.38.Bx, 14.20.Dh

I. INTRODUCTION

Deeply virtual Compton scattering (DVCS), $\gamma^*(q) + p(P) \to \gamma(q') + p(P')$, where the virtuality of the initial photon $Q^2 = -q^2$ is large, provides a valuable probe of the elementary quark structure of the target proton near the light cone. At leading twist, QCD factorization applies [1], and each DVCS helicity amplitude factorizes as a convolution in x of the hard $\gamma^* q \to \gamma q$ Compton amplitude with a hadronic subamplitude constructed from the generalized parton distributions (GPDs) $H(x, \zeta, t)$, $E(x, \zeta, t)$, $\tilde{H}(x, \zeta, t)$ and $\tilde{E}(x, \zeta, t)$. Here x is the light-cone momentum fraction of the struck quark; the skewness $\zeta = \frac{Q^2}{2P \cdot q}$ measures the longitudinal momentum transfer in the DVCS process.

Measurements of the momentum and spin dependence of the DVCS process in $e^\pm p \to \gamma e^\pm p$ can provide a remarkable window to the QCD structure of hadrons at the amplitude level. The interference of the DVCS amplitude and the coherent Bethe-Heitler amplitude leads to an $e^\pm$ asymmetry which is related to the real part of the DVCS amplitude [2]. The imaginary part can also be accessed through various spin asymmetries [3]. In the forward limit of zero momentum transfer, the GPDs reduce to ordinary parton distributions; on the other hand, the integration of GPDs over x reduces them to electromagnetic and gravitational form factors.

The DVCS helicity amplitudes can be constructed in light-cone gauge from the overlap of the target hadron's light-front wave functions (LFWFs) [4,5]. Since the DVCS process involves off-forward hadronic matrix elements of light-front bilocal currents, the overlaps are, in general, nondiagonal in particle number, unlike ordinary parton distributions. Thus in the case of GPDs, one requires not only the diagonal parton number conserving $n \to n$ overlap of the initial and final light-front wave functions, but also an off-diagonal $n + 1 \to n - 1$ overlap, where the parton number is decreased by 2. Thus the GPDs measure hadron structure at the amplitude level in contrast to the probabilistic properties of parton distribution functions.

The GPDs have become objects of much theoretical as well as experimental attention since they provide a rich source of information of hadron structure. Burkardt has noted that a Fourier transform (FT) of the GPDs with respect to the transverse momentum transfer $\Delta_\perp$ in the idealized limit $\zeta = 0$ measures the impact parameter dependent parton distributions $q(x, b_\perp)$ defined from the absolute squares of the hadron's light-front wave functions (LFWFs) in x and impact space [6,7]. The impact representation on the light front was first introduced by Soper [8] in the context of the FT of the elastic form factor (see Appendix A). The function $q(x, b_\perp)$ is defined for a hadron

with sharp plus momentum P^+, localized in the transverse plane, such that the transverse center of momentum vanishes, $R_\perp = 0$. (One can also work with a wave packet localized in the transverse position space in order to avoid a state normalized to a δ function.) Thus $q(x, b_\perp)$ gives simultaneous information on the distributions of a quark as a function of the longitudinal light-front momentum fraction $x = k^+/P^+ = (k^0 + k^3)/(P^0 + P^3)$ and the transverse distance $b_\perp$ of the parton from the center of the proton in the transverse plane. We use the standard LF coordinates $P^\pm = P^0 \pm P^3$, $y^\pm = y^0 \pm y^3$. Since the proton is on shell, $P^+P^- - P_\perp^2 = M_p^2$.

Since the incoming photon is spacelike ($q^2 < 0$) and the final photon is on shell ($q'^2 = 0$), the skewness ζ is never zero in a physical experiment. In this paper, we will investigate the DVCS amplitude in the longitudinal position space by taking the FT with respect to ζ. We show that the FT of the DVCS amplitude in ζ reveals the structure of a hadron target in a longitudinal impact parameter space. Thus, our work is suited for the direct analysis of experimental data and is complementary to the work of Burkardt and Soper. Physically, the FT of the DVCS amplitude allows one to measure the correlation within the hadron between the incoming and outgoing quark currents at transverse separation $b_\perp$ and longitudinal separation $\sigma = b^-P^+/2$ at fixed light-front time $\tau = z + t/c$. Since Lorentz boosts are kinematical in the front form, the correlation determined in the three-dimensional $b_\perp$, σ space is frame independent.

Even though light-front dynamics was proposed by Dirac [9] more than 50 years ago, and the utility of the light-front momentum fraction $x = k^+/P^+$ dates to the inception of the Feynman parton model, very little is known about the longitudinal coordinate space structure of hadron wave functions and related physical observables. To the best of our knowledge, the first work to investigate this subject is Ref. [10] where it is shown that by Fourier transforming the form factors one observes profiles in b^- with kinks and antikinks. In addition to the light-front longitudinal structure of DVCS amplitudes in one-loop QED and meson models, we also present the corresponding structure of the LFWFs of the quantum fluctuations of a lepton to order e^2 in QED.

Burkardt [6] has noted the possibility of taking the FT with respect to the longitudinal momentum of the active quark. However, since the GPDs depend on a sharp x, the Heisenberg uncertainty relation severely restricts the longitudinal position space interpretation of GPDs. In contrast, we will deal directly with DVCS amplitudes which are integrated over x and take the FT with respect to the longitudinal momentum *transfer*.

It has been shown in [11] that one can define a quantum mechanical Wigner distribution for the relativistic quarks and gluons inside the proton. Integrating over k^- and $k^\perp$, one obtains a four-dimensional quantum distribution which is a function of $\vec{r}$ and k^+, where $\vec{r}$ is the quark phase space position defined in the rest frame of the proton. These distributions are related to the FT of GPDs in the same frame. However, the Wigner distributions cannot be measured experimentally.

In contrast, we will study the observable DVCS amplitudes directly in longitudinal position space. We shall show that the Fourier transforms of the DVCS amplitudes in the variable $\sigma = b^-P^+/2$, where the three-dimensional coordinate $\vec{b} = (b_\perp, b^-)$ is conjugate to the momentum transfer $\vec{\Delta}$, provide a light-front image of the target hadron in a frame-independent three-dimensional light-front coordinate space. We find that, in the models studied, the Fourier transforms of the DVCS amplitudes exhibit diffraction patterns. The results are analogous to the diffractive scattering of a wave in optics where the distribution in σ measures the physical size of the scattering center in a one-dimensional system.

A summary of our main results has been given in [12]. In this paper we will present a detailed analysis and provide several additional results.

In order to illustrate the general framework, we will present an explicit calculation of the FT of the DVCS on a fermion in QED at one-loop order [13]. In effect, we shall represent a spin-$\frac{1}{2}$ system as a composite of a spin-$\frac{1}{2}$ fermion and a spin-1 vector boson, with arbitrary masses [4]. This one-loop model is self-consistent since it has the correct interrelation of different Fock components of the state as given by the light-front eigenvalue equation [14]. In particular, its two- and three-body Fock components can be obtained analytically from QED. This model has been used to calculate the spin and orbital angular momentum of a composite relativistic system [15] as well as the GPDs in the impact parameter space [16,17]. The calculation is thus exact to $O(\alpha)$, and it gives the Schwinger anomalous magnetic moment, the corresponding electron's Dirac and Pauli form factors [15,16], as well as the correct gravitational form factors, including the vanishing of the anomalous gravitomagnetic moment $B(0)$ in agreement with the equivalence theorem [18]. In addition, it provides a template for the wave functions of an effective quark-diquark model of the valence Fock state of the proton light-front wave function.

Deep inelastic scattering structure functions and their connection to the spin and orbital angular momentum of the nucleon have been addressed for a dressed quark state in light-front QCD in [19,20] using a similar Fock space expansion of the state. This approach has also been used to investigate the twist-three GPDs in [21]. We will also present here numerical results for a simulated model for a mesonlike hadron, which we obtain by taking a derivative of the dressed electron LFWF with respect to the bound-state mass M, thus improving the behavior of the wave function towards the end points in x. In this model, the DVCS amplitude is purely real. A similar power-law

LFWF has been used in [22] to construct the GPDs for a meson.

In principle, the LFWFs of hadrons in QCD can be computed using a nonperturbative method such as discretized light-cone quantization (DLCQ), where the LF Hamiltonian is diagonalized on a free Fock basis [14]. This has been accomplished for simple confining quantum field theories such as QCD (1 + 1) [23].

Models for the LFWFs of hadrons in (3 + 1) dimensions displaying confinement at large distances and conformal symmetry at short distances have been obtained using the AdS/CFT method [24]. We will also present the LFWFs in this hadron model in invariant three-dimensional coordinate space by Fourier transforming in both x and $k^\perp$.

The plan of the paper is as follows: Sec. II summarizes the kinematics of the DVCS process. In Sec. III we give the analytic expressions for the DVCS amplitude and its explicit formulas in QED at one loop. The calculation of the Fourier transform of the DVCS amplitude for an electron target at one loop is given in Sec. IV. The simulated hadron model is discussed in Sec. V. We then derive the DVCS amplitudes using a model meson LFWF as obtained from holographic QCD in Sec. VI. A summary and the conclusions are given in Sec. VII.

II. KINEMATICS

The kinematics of the DVCS process has been given in detail in [4,5]. One can work in a frame where the momenta of the initial and final proton has a $\Delta \to -\Delta$ symmetry [4]; however, in this frame, the kinematics in terms of the parton momenta becomes more complicated. Here, we shall use the frame of Ref. [4]. The momenta of the initial and final proton are given by

$$P = \left(P^+, \vec{0}_\perp, \frac{M^2}{P^+}\right), \tag{2.1}$$

$$P' = \left((1-\zeta)P^+, -\vec{\Delta}_\perp, \frac{M^2 + \vec{\Delta}_\perp^2}{(1-\zeta)P^+}\right), \tag{2.2}$$

where M is the proton mass. The four-momentum transfer from the target is

$$\Delta = P - P' = \left(\zeta P^+, \vec{\Delta}_\perp, \frac{t + \vec{\Delta}_\perp^2}{\zeta P^+}\right), \tag{2.3}$$

where $t = \Delta^2$. In addition, overall energy-momentum conservation requires $\Delta^- = P^- - P'^-$, which connects $\vec{\Delta}_\perp^2$, ζ, and t according to

$$t = 2P\cdot\Delta = -\frac{\zeta^2 M^2 + \vec{\Delta}_\perp^2}{1-\zeta}. \tag{2.4}$$

The coordinate b conjugate to Δ is defined by $b\cdot\Delta = \frac{1}{2}b^+\Delta^- + \frac{1}{2}b^-\Delta^+ - b_\perp\cdot\Delta_\perp$. We also define the boost-invariant variable $\sigma = b^- P^+/2$ so that $\frac{1}{2}b^-\Delta^+ = \frac{1}{2}b^- P^+\zeta = \sigma\zeta$. Thus σ is an "impact parameter" but in the boost-invariant longitudinal coordinate space.

It is convenient to choose a frame where the incident spacelike photon carries $q^+ = 0$ so that $q^2 = -Q^2 = -\vec{q}_\perp^2$ (however, it is not mandatory to choose this frame):

$$q = \left(0, \vec{q}_\perp, \frac{(\vec{q}_\perp + \vec{\Delta}_\perp)^2}{\zeta P^+} + \frac{\zeta M^2 + \vec{\Delta}_\perp^2}{(1-\zeta)P^+}\right), \tag{2.5}$$

$$q' = \left(\zeta P^+, \vec{q}_\perp + \vec{\Delta}_\perp, \frac{(\vec{q}_\perp + \vec{\Delta}_\perp)^2}{\zeta P^+}\right). \tag{2.6}$$

We will be interested in deeply virtual Compton scattering, where Q^2 is large compared to the masses and $-t$. Then, we have

$$\frac{Q^2}{2P\cdot q} = \zeta \tag{2.7}$$

up to corrections in $1/Q^2$. Thus ζ plays the role of the Bjorken variable in deeply virtual Compton scattering. For a fixed value of $-t$, the allowed range of ζ is given by

$$0 \le \zeta \le \frac{(-t)}{2M^2}\left(\sqrt{1 + \frac{4M^2}{(-t)}} - 1\right). \tag{2.8}$$

III. DEEPLY VIRTUAL COMPTON SCATTERING

The virtual Compton amplitude $M^{\mu\nu}(\vec{q}_\perp, \vec{\Delta}_\perp, \zeta)$, i.e., the transition matrix element of the process $\gamma^*(q) + p(P) \to \gamma(q') + p(P')$, can be defined from the light-cone time-ordered product of currents

$$M^{\mu\nu}(\vec{q}_\perp, \vec{\Delta}_\perp, \zeta) = i\int d^4y e^{-iq\cdot y}\langle P'|TJ^\mu(y)J^\nu(0)|P\rangle, \tag{3.1}$$

where the Lorentz indices μ and ν denote the polarizations of the initial and final photons, respectively. In the limit $Q^2 \to \infty$ at fixed ζ and t the Compton amplitude is thus given by

$$\begin{aligned} M^{IJ}(\vec{q}_\perp, \vec{\Delta}_\perp, \zeta) &= \epsilon_\mu^I \epsilon_\nu^{*J} M^{\mu\nu}(\vec{q}_\perp, \vec{\Delta}_\perp, \zeta) \\ &= -e_q^2 \frac{1}{2\bar{P}^+}\int_{\zeta-1}^1 dz \Big\{ t^{IJ}(z,\zeta)\bar{U}(P') \\ &\quad \times \Big[H(z,\zeta,t)\gamma^+ + E(z,\zeta,t)\frac{i}{2M} \\ &\quad \times \sigma^{+\alpha}(-\Delta_\alpha)\Big] U(P)\Big\}, \end{aligned} \tag{3.2}$$

where $\bar{P} = \frac{1}{2}(P' + P)$. For simplicity we only consider one

quark with flavor q and electric charge e_q. Here we consider the contribution of only the spin-independent GPDs H and E. Throughout our analysis we will assume the Born approximation to the photon-quark amplitude; i.e., the ''handbag'' approximation, corresponding to setting the Wilson line to 1 in light-cone gauge. In principle, there can be rescattering corrections in the light-cone gauge between the spectators at leading twist analogous to those which occur in diffractive deep inelastic scattering [25], but these will not be considered here.

For circularly polarized initial and final photons (I, J are $\uparrow$ or $\downarrow$) we have

$$t^{\uparrow\uparrow}(z,\zeta) = t^{\downarrow\downarrow}(z,\zeta) = \frac{1}{z-i\epsilon} + \frac{1}{z-\zeta+i\epsilon}, \qquad t^{\uparrow\downarrow}(z,\zeta) = t^{\downarrow\uparrow}(z,\zeta) = 0. \tag{3.3}$$

The two photon polarization vectors in light-cone gauge are given by

$$\epsilon^{\uparrow,\downarrow} = \left(0, \vec{\epsilon}_\perp^{\uparrow,\downarrow}, \frac{\vec{\epsilon}_\perp^{\uparrow,\downarrow}\cdot\vec{k}_\perp}{2k^+}\right), \qquad \vec{\epsilon}_\perp^{\uparrow,\downarrow} = \mp\frac{1}{\sqrt{2}}\begin{pmatrix}1\\ \pm i\end{pmatrix}, \tag{3.4}$$

where k denotes the appropriate photon momentum. The polarization vectors satisfy the Lorentz condition $k\cdot\epsilon = 0$. For a longitudinally polarized initial photon, the Compton amplitude is of order $1/Q$ and thus vanishes in the limit $Q^2 \to \infty$. At order $1/Q$ there are several corrections to the simple structure in Eq. (3.2). We do not consider them here.

The generalized parton distributions H, E are defined through matrix elements of the bilinear vector and axial vector currents on the light cone:

$$\int \frac{dy^-}{8\pi} e^{izP^+y^-/2}\langle P'|\bar{\psi}(0)\gamma^+\psi(y)|P\rangle|_{y^+=0,y_\perp=0} = \frac{1}{2\bar{P}^+}\bar{U}(P')\Big[H(z,\zeta,t)\gamma^+ + E(z,\zeta,t) \times \frac{i}{2M}\sigma^{+\alpha}(-\Delta_\alpha)\Big]U(P). \tag{3.5}$$

The off-forward matrix elements given by Eq. (3.5) can be expressed in terms of overlaps of LFWFs of the state [4,5]. We now calculate the matrix elements in terms of the LFWFs. For this, we take the state to be an electron in QED at one loop and consider the LFWFs for this system.

DVCS in QED at one loop

The light-front Fock state wave functions corresponding to the quantum fluctuations of a physical electron can be systematically evaluated in QED perturbation theory. The light-cone time-ordered contribution for the state to the DVCS amplitude are given in Fig. 6 of [4]. The state is expanded in Fock space, giving contributions from $|e^-\gamma\rangle$ and $|e^-e^-e^+\rangle$, in addition to renormalizing the one-electron state. The two-particle state is expanded as

$$|\Psi^\uparrow_{\text{two particle}}(P^+,\vec{P}_\perp=\vec{0}_\perp)\rangle = \int \frac{dx d^2\vec{k}_\perp}{\sqrt{x(1-x)}16\pi^3}\Big[\psi^\uparrow_{+(1/2)+1}(x,\vec{k}_\perp)\Big|+\frac{1}{2}+1;xP^+,\vec{k}_\perp\Big\rangle + \psi^\uparrow_{+\frac{1}{2}-1}(x,\vec{k}_\perp)\Big|+\frac{1}{2}-1;xP^+,\vec{k}_\perp\Big\rangle + \psi^\uparrow_{-(1/2)+1}(x,\vec{k}_\perp)\Big|-\frac{1}{2}+1;xP^+,\vec{k}_\perp\Big\rangle + \psi^\uparrow_{-(1/2)-1}(x,\vec{k}_\perp)\Big|-\frac{1}{2}-1;xP^+,\vec{k}_\perp\Big\rangle\Big], \tag{3.6}$$

where the two-particle states $|s_f^z, s_b^z; x, \vec{k}_\perp\rangle$ are normalized as in [4]. Here s_f^z and s_b^z denote the z component of the spins of the constituent fermion and boson, respectively, and the variables x and $\vec{k}_\perp$ refer to the momentum of the fermion. The light-cone momentum fraction $x_i = \frac{k_i^+}{P^+}$ satisfies $0 < x_i \le 1$, $\sum_i x_i = 1$. We employ the light-cone gauge $A^+ = 0$, so that the gauge boson polarizations are physical. The three-particle state has a similar expansion. Both the two- and three-particle Fock state components are given in [4]. The two-particle wave functions for spin-up electrons are [4,13,15]

$$\begin{Bmatrix} \psi^\uparrow_{+(1/2)+1}(x,\vec{k}_\perp) = -\sqrt{2}\frac{-k^1+ik^2}{x(1-x)}\varphi, \\ \psi^\uparrow_{+(1/2)-1}(x,\vec{k}_\perp) = -\sqrt{2}\frac{k^1+ik^2}{1-x}\varphi, \\ \psi^\uparrow_{-(1/2)+1}(x,\vec{k}_\perp) = -\sqrt{2}\Big(M-\frac{m}{x}\Big)\varphi, \\ \psi^\uparrow_{-(1/2)-1}(x,\vec{k}_\perp) = 0, \end{Bmatrix}, \tag{3.7}$$

$$\varphi(x,\vec{k}_\perp) = \frac{e}{\sqrt{1-x}}\frac{1}{M^2 - \frac{\vec{k}_\perp^2+m^2}{x} - \frac{\vec{k}_\perp^2+\lambda^2}{1-x}}. \tag{3.8}$$

Similarly, the wave function for an electron with negative helicity can also be obtained.

Following Refs. [4,13,15], we work in a generalized form of QED by assigning a mass M to the external electrons, a distinct mass m for the internal electron lines, and a nonzero mass λ for the internal photon lines, assuming the stability condition $M < m + \lambda$. This provides a model for a composite fermion state with mass M with fermion and vector "diquark" constituents. The electron in QED also has a one-particle component

$$|\Psi^{\uparrow,\downarrow}_{\text{one particle}}(P^+, \vec{P}_\perp = \vec{0}_\perp)\rangle = \int \frac{dx d^2\vec{k}_\perp}{\sqrt{x}16\pi^3} 16\pi^3 \delta(1-x)\delta^2(\vec{k}_\perp)\psi_{(1)} \left| \pm\frac{1}{2}; xP^+, \vec{k}_\perp \right\rangle, \tag{3.9}$$

where the single-constituent wave function is given by

$$\psi_{(1)} = \sqrt{Z}. \tag{3.10}$$

Here $\sqrt{Z}$ is the wave-function renormalization of the one-particle state and ensures overall probability conservation. Since we are working to $\mathcal{O}(\alpha)$, we can set $Z = 1$ in the $3 \to 1$ wave-function overlap contributions. At $x = 1$, there are contributions from the overlap of one-particle states which depend on Z. We have imposed a cutoff on x near this point. Also, in order to regulate the ultraviolet divergences, one has to introduce a regulator. Here, we use a cutoff Λ on the transverse momentum $k^\perp$ as a regulator.

In the domain $\zeta < z < 1$, there are diagonal $2 \to 2$ overlap contributions to Eq. (3.5), both helicity flip, F^{22}_{+-} ($\lambda' \neq \lambda$), and helicity nonflip, F^{22}_{++} ($\lambda' = \lambda$) [4]. The GPDs $H_{(2\to2)}(z, \zeta, t)$ and $E_{(2\to2)}(z, \zeta, t)$ are zero in the domain $\zeta - 1 < z < 0$, which corresponds to emission and reabsorption of an e^+ from a physical electron. Contributions to $H_{(n\to n)}(z, \zeta, t)$ and $E_{(n\to n)}(z, \zeta, t)$ in that domain only appear beyond one-loop level since the DVCS amplitude contains integrations over z, y^-, and x. When the integration over y^- is performed, the fermion part of the bilocal current yields a factor $\delta(z - x)$ and the antifermion part of the bilocal current yields a factor $\delta(z + x)$. The latter contribution is absent in the one-loop DVCS amplitude of a electron target, which we consider in the present work.

We have

$$\begin{aligned} F^{22}_{++} &= \frac{\sqrt{1-\zeta}}{1-\frac{\zeta}{2}} H_{(2\to2)}(x, \zeta, t) - \frac{\zeta^2}{4(1-\frac{\zeta}{2})\sqrt{1-\zeta}} E_{(2\to2)}(x, \zeta, t) \\ &= \int \frac{d^2\vec{k}_\perp}{16\pi^3} [\psi^{\uparrow *}_{+(1/2)+1}(x', \vec{k}'_\perp)\psi^{\uparrow}_{+(1/2)+1}(x, \vec{k}_\perp) + \psi^{\uparrow *}_{+(1/2)-1}(x', \vec{k}'_\perp)\psi^{\uparrow}_{+(1/2)-1}(x, \vec{k}_\perp) + \psi^{\uparrow *}_{-(1/2)+1}(x', \vec{k}'_\perp)\psi^{\uparrow}_{-(1/2)+1}(x, \vec{k}_\perp)], \end{aligned} \tag{3.11}$$

$$\begin{aligned} F^{22}_{+-} &= \frac{1}{\sqrt{1-\zeta}} \frac{(\Delta^1 - i\Delta^2)}{2M} E_{(2\to2)}(x, \zeta, t) \\ &= \int \frac{d^2\vec{k}_\perp}{16\pi^3} [\psi^{\uparrow *}_{+(1/2)-1}(x', \vec{k}'_\perp)\psi^{\downarrow}_{+(1/2)-1}(x, \vec{k}_\perp) + \psi^{\uparrow *}_{-(1/2)+1}(x', \vec{k}'_\perp)\psi^{\downarrow}_{-(1/2)+1}(x, \vec{k}_\perp)], \end{aligned} \tag{3.12}$$

where

$$x' = \frac{x-\zeta}{1-\zeta}, \qquad \vec{k}'_\perp = \vec{k}_\perp - \frac{1-x}{1-\zeta}\vec{\Delta}_\perp. \tag{3.13}$$

Using the explicit form of the two-particle wave functions, we obtain

$$\begin{aligned} F^{22}_{++} &= \frac{e^2}{16\pi^3} \frac{1}{(1-x)} \frac{[(1-\zeta) + x(x-\zeta)]}{\sqrt{1-\zeta}} [I^{NF}_1 + I^{NF}_2 + [B(x, \zeta) + M^2 x(1-x) - m^2(1-x) - \lambda^2 x] I^{NF}_3] \\ &\quad + \frac{e^2}{8\pi^3} \left(\frac{M}{1-\zeta} - \frac{m}{x-\zeta}\right)\left(M - \frac{m}{x}\right) \frac{x(1-x)(x-\zeta)}{\sqrt{1-\zeta}} I^{NF}_3. \end{aligned} \tag{3.14}$$

We use the notation

$$L_1 = (k^\perp)^2 - 2k^\perp \cdot \Delta^\perp \frac{(1-x)}{(1-\zeta)} - B(x, \zeta), \qquad L_2 = (k^\perp)^2 - M^2 x(1-x) + m^2(1-x) + \lambda^2 x \tag{3.15}$$

and $B(x,\zeta) = \frac{M^2(1-x)(x-\zeta)}{(1-\zeta)^2} - \frac{(\Delta^\perp)^2(1-x)^2}{(1-\zeta)^2} - m^2\frac{(1-x)}{(1-\zeta)} - \lambda^2\frac{(x-\zeta)}{(1-\zeta)}$. The integrals are given by

$$
\begin{aligned}
I_1^{NF} &= \int \frac{d^2k^\perp}{L_1} = \pi \log\Big[\frac{\Lambda^2}{|B(x,\zeta)|}\Big],\\
I_2^{NF} &= \int \frac{d^2k^\perp}{L_2} = \pi \log\Big[\frac{\Lambda^2}{|-M^2x(1-x)+m^2(1-x)+\lambda^2 x|}\Big],\\
I_3^{NF} &= \int \frac{d^2k^\perp}{L_1L_2} = \pi\int_0^1 d\beta \frac{1}{D(x,\zeta,\beta)},
\end{aligned}
\tag{3.16}
$$

where $D(x,\zeta,\beta) = \beta m^2(1-x) - \beta M^2 x(1-x) + \beta\lambda^2 x - (1-\beta)B(x,\zeta) - (1-\beta)^2(1-x')^2(\Delta^\perp)^2$. Here Λ is the cutoff on the transverse momentum $k^\perp$ and $x' = \frac{(x-\zeta)}{(1-\zeta)}$.

The helicity-flip part can be written as

$$
F_{+-}^{22} = \frac{e^2}{8\pi^3}\Big[\frac{x(x-\zeta)}{\sqrt{1-\zeta}}\Big(M-\frac{m}{x}\Big)I_1^F - \Big(M-\frac{m}{x}\Big)\frac{x(1-x)(x-\zeta)}{(1-\zeta)^{3/2}}I_2^F\Big] - \frac{e^2}{8\pi^3}\Big(\frac{M}{1-\zeta}+\frac{m}{\zeta-x}\Big)\frac{x(x-\zeta)}{\sqrt{1-\zeta}}I_1^F, \tag{3.17}
$$

where $I_1^F = \int \frac{d^2k^\perp k_V^\perp}{L_1L_2}$ and $I_2^F = \int \frac{d^2k^\perp \Delta_V^\perp}{L_1L_2}$. We have used the notation $A_V^\perp = A^1 - iA^2$. These integrals can be done using the method described in Sec. III of Ref. [17] and we obtain

$$
I_1^F = \pi\int_0^1 dy \frac{y(1-x')\Delta_V^\perp}{Q(x,\zeta,y)}, \tag{3.18}
$$

where $Q(x,\zeta,y) = (1-y)[-M^2x(1-x)+m^2(1-x)+\lambda^2x] - yB(x,\zeta) - y^2(1-x')^2(\Delta_\perp)^2$ and

$$
I_2^F = \pi\int_0^1 \frac{dy\Delta_V^\perp}{Q(x,\zeta,y)}. \tag{3.19}
$$

The scale Λ dependence is suppressed in F_{+-}^{22}.

The contribution in the domain, $0 < z < \zeta$, comes from an overlap of three-particle and one-particle LFWFs. When the electron's helicity is not flipped, this contribution is given by [4]

$$
\begin{aligned}
F_{++}^{31} &= \frac{\sqrt{1-\zeta}}{1-\frac{\zeta}{2}}H_{(3\to1)}(x,\zeta,t) - \frac{\zeta^2}{4(1-\frac{\zeta}{2})\sqrt{1-\zeta}}E_{(3\to1)}(x,\zeta,t)\\
&= \sqrt{1-\zeta}\int\frac{\mathrm{d}^2\vec{k}_\perp}{16\pi^3}[\psi^\uparrow_{+(1/2)+(1/2)-(1/2)}(x,1-\zeta,\zeta-x,\vec{k}_\perp,-\vec{\Delta}_\perp,\vec{\Delta}_\perp-\vec{k}_\perp)\\
&\quad + \psi^\uparrow_{-(1/2)+(1/2)+(1/2)}(x,1-\zeta,\zeta-x,\vec{k}_\perp,-\vec{\Delta}_\perp,\vec{\Delta}_\perp-\vec{k}_\perp)],
\end{aligned}
\tag{3.20}
$$

and can be written as, using the three-particle wave function,

$$
\begin{aligned}
F_{++}^{31} &= \frac{e^2}{8\pi^3}(1-\zeta-\zeta x+x^2)\frac{x\sqrt{1-\zeta}}{\zeta(1-x)}\Big[\frac{1}{(1-x)}J_1^{INF} - \frac{1}{(1-\zeta)}J_2^{INF}\Big]\\
&\quad - \frac{e^2}{8\pi^3}\frac{\sqrt{1-\zeta}x^2(\zeta-x)}{\zeta}\Big(M-\frac{m}{x}\Big)\Big(\frac{M}{(1-\zeta)}+\frac{m}{(\zeta-x)}\Big)J_3^{INF},
\end{aligned}
\tag{3.21}
$$

with

$$
\begin{aligned}
J_1^{INF} &= J_2^{NF} + [M^2x(1-x) - m^2(1-x) - \lambda^2x]J_3^{NF},\\
J_2^{INF} &= \frac{\zeta}{2x}[J_2^{NF} - J_1^{NF} + [M^2x(1-x) - m^2(1-x)\\
&\quad - \lambda^2x + A(x,\zeta)]J_3^{NF}],\\
J_3^{INF} &= J_3^{NF}.
\end{aligned}
\tag{3.22}
$$

We denote

$$
\begin{aligned}
l_1 &= (k^\perp)^2 - M^2x(1-x) + m^2(1-x) + \lambda^2x,\\
l_2 &= (k^\perp)^2 - 2k^\perp\cdot\Delta^\perp\frac{x}{\zeta} + A(x,\zeta),
\end{aligned}
\tag{3.23}
$$

and $A(x,\zeta) = \frac{1}{\zeta(1-\zeta)}[x(1-x)(\Delta^\perp)^2 + m^2\zeta(1-\zeta) + x\zeta(\zeta-x)M^2]$. The integrals can be written as

$$J_1^{NF} = \int \frac{d^2k^\perp}{l_1} = \pi \log\left[\frac{\Lambda^2}{|-M^2x(1-x)+m^2(1-x)+\lambda^2 x|}\right],$$
$$J_2^{NF} = \int \frac{d^2k^\perp}{l_2} = \pi \log\left[\frac{\Lambda^2}{|A(x,\zeta)|}\right], \tag{3.24}$$
$$J_3^{NF} = \int \frac{d^2k^\perp}{l_1 l_2} = \pi \int_0^1 d\beta \frac{1}{C(x,\zeta,\beta)},$$

where $C(x,\zeta,\beta) = -\beta M^2 x(1-x) + \beta m^2(1-x) + \beta\lambda^2 x + (1-\beta)A(x,\zeta) - (1-\beta)^2 \frac{x^2}{\zeta^2}\Delta_\perp^2$.

The helicity-flip part is given by [4]

$$F^{31}_{+-} = \frac{1}{\sqrt{1-\zeta}} \frac{(\Delta^1 - i\Delta^2)}{2M} E_{(3\to 1)}(x,\zeta,t)$$
$$= \sqrt{1-\zeta}\int \frac{\mathrm{d}^2\vec{k}_\perp}{16\pi^3}[\psi^\downarrow_{+(1/2)+(1/2)-(1/2)}(x,1-\zeta,\zeta-x,\vec{k}_\perp,-\vec{\Delta}_\perp,\vec{\Delta}_\perp-\vec{k}_\perp)$$
$$+ \psi^\downarrow_{-(1/2)+(1/2)+(1/2)}(x,1-\zeta,\zeta-x,\vec{k}_\perp,-\vec{\Delta}_\perp,\vec{\Delta}_\perp-\vec{k}_\perp)]. \tag{3.25}$$

Using the three-particle wave function, this can be written as

$$F^{31}_{+-} = \frac{e^2}{8\pi^3}\sqrt{1-\zeta}\left(M-\frac{m}{x}\right)\frac{x^2(\zeta-x)}{\zeta}\left[\frac{1}{(1-\zeta)}J_2^F - \frac{1}{(1-x)}J_1^F\right]$$
$$+ \frac{e^2}{8\pi^3}\sqrt{1-\zeta}\left[\frac{M}{(1-\zeta)}+\frac{m}{(\zeta-x)}\right]\frac{x^2(\zeta-x)}{\zeta}\frac{1}{(1-x)}J_1^F, \tag{3.26}$$

where

$$J_1^F = \int \frac{d^2k^\perp k_V^\perp}{l_1 l_2} = \pi\int_0^1 dy \frac{(1-y)\Delta_V^\perp \frac{x}{\zeta}}{P(x,\zeta,y)}, \qquad J_2^F = \int \frac{d^2k^\perp \Delta_V^\perp}{l_1 l_2} = \pi\int_0^1 dy \frac{\Delta_V^\perp}{P(x,\zeta,y)}, \tag{3.27}$$

with $P(x,\zeta,y) = (1-y)A(x,\zeta) - (1-y)^2\frac{x^2}{\zeta^2}\times(\Delta^\perp)^2 + y[-M^2x(1-x)+m^2(1-x)+\lambda^2 x]$.

We calculate the DVCS amplitude given by Eq. (3.2) using the off-forward matrix elements calculated above. The real and imaginary parts are calculated separately using the prescription

$$\int_0^1 dx \frac{1}{x-\zeta+i\epsilon}F(x,\zeta)$$
$$= P\int_0^1 dx \frac{1}{x-\zeta}F(x,\zeta) - i\pi F(\zeta,\zeta). \tag{3.28}$$

Here P denotes the principal value defined as

$$P\int_0^1 dx \frac{1}{x-\zeta}F(x,\zeta) = \lim_{\epsilon\to 0}\left[\int_0^{\zeta-\epsilon}\frac{1}{x-\zeta}F(x,\zeta) + \int_{\zeta+\epsilon}^1 \frac{1}{x-\zeta}F(x,\zeta)\right], \tag{3.29}$$

where

$$F(x,\zeta) = F^{31}_{ij}(x,\zeta,\Delta_\perp), \quad \text{for } 0<x<\zeta$$
$$= F^{22}_{ij}(x,\zeta,\Delta_\perp), \quad \text{for } \zeta<x<1$$

with $ij = ++$ for helicity nonflip and $ij = +-$ for helicity-flip amplitudes. Since the off-forward matrix elements are continuous at $x=\zeta$, $F(\zeta,\zeta) = F^{22}_{ij}(x=\zeta,\zeta,\Delta_\perp) = F^{31}_{ij}(x=\zeta,\zeta,\Delta_\perp)$. Note that, for an electron state, the contribution vanishes for $x<0$ and the principal value prescription cannot be used at $x=0$. The off-forward matrix elements F^{31} (which contribute in the kinematical region $0<x<\zeta$) vanish as $x\to 0$; as a result, there is no logarithmic divergence at this point for nonzero ζ. But, we need to be careful here as, when we consider the Fourier transform in σ space, ζ can go to zero and divergences from small x can occur from F^{22} which is finite and nonzero at $x,\zeta\to 0$.

The imaginary part of the amplitude when the electron helicity is not flipped is then given by

$$\mathrm{Im}[M_{++}](\zeta,\Delta_\perp) = \pi e^2 F^{22}_{++}(x=\zeta,\zeta,\Delta_\perp). \tag{3.30}$$

A similar expression holds in the case when the electron helicity is flipped ($\mathrm{Im}[M_{+-}](\zeta,\Delta^\perp)$) in which F_{++} are replaced by F_{+-}. The helicity-flip DVCS amplitude is proportional to $(\Delta_1 - i\Delta_2)$ as seen from Eqs. (3.17) and (3.26). In the numerical results for the helicity-flip pro-

cesses that we present here, for simplicity we have taken $\Delta_2 = 0$. The imaginary part receives contributions from $x = \zeta$. The off-forward matrix elements are continuous at $x = \zeta$, and in Eq. (3.30) we have used this continuity. The other regions of x contribute to the real part. It is to be emphasized that we are using the handbag approximation of the DVCS amplitude. Contributions from the Wilson lines are, in general, not zero, and they can give rise to new phase structures as seen in single-spin asymmetries [26].

The real part of the DVCS amplitude is given by

$$\mathrm{Re}\,[M_{++}](\zeta, \Delta_\perp) = -e^2 \int_\epsilon^{\zeta-\epsilon_1} dx F^{31}_{++}(x, \zeta, \Delta_\perp)\left[\frac{1}{x} + \frac{1}{x-\zeta}\right] - e^2 \int_{\zeta+\epsilon_1}^{1-\epsilon} dx F^{22}_{++}(x, \zeta, \Delta_\perp)\left[\frac{1}{x} + \frac{1}{x-\zeta}\right]. \tag{3.31}$$

A similar expression holds for the helicity-flip DVCS amplitude.

The energy dependence of the DVCS amplitude at the high energies $s \gg Q^2, -t$ can be deduced up to logarithms using Regge analysis. In our QED model for DVCS, two spin $1/2$ propagators are exchanged in the t channel. This implies Regge behavior $s^{\alpha(0)}$, where $\alpha(0) = j_1 + j_2 - 1 = 0$. Thus, up to logarithms, the DVCS amplitude has no dependence on the initial energy of the incident electron and photon.

IV. CALCULATION OF THE FOURIER TRANSFORM

In order to obtain the DVCS amplitude in b^- space, we take a Fourier transform in ζ as

$$\begin{aligned} A_{++}(\sigma, t) &= \frac{1}{2\pi}\int_{\epsilon_2}^{1-\epsilon_2} d\zeta e^{i\sigma\zeta} M_{++}(\zeta, \Delta_\perp), \\ A_{+-}(\sigma, t) &= \frac{1}{2\pi}\int_{\epsilon_2}^{1-\epsilon_2} d\zeta e^{i\sigma\zeta} M_{+-}(\zeta, \Delta_\perp), \end{aligned} \tag{4.1}$$

where $\sigma = \frac{1}{2}P^+ b^-$ is the boost-invariant longitudinal distance on the light cone. The spatial properties of deep inelastic scattering obtained from a Fourier transform of structure functions from $x = k^+/P^+$ to b^- space have been discussed by Hoyer [27]. In Fig. 1 we show the handbag diagram of the DVCS amplitude in coordinate space, which is similar to Fig. 10 of the above reference.

Both real and imaginary parts of the DVCS amplitude are obtained separately. The real part of the amplitude depends on the cutoffs. Since the off-forward matrix elements are continuous at $x = \zeta$, the DVCS amplitude is independent of the cutoff ϵ_1. The cutoffs have to be chosen such that $\epsilon_2 - \epsilon_1 \geq \epsilon$, $\epsilon_2 + \epsilon_1 < 1 - \epsilon$, in order to have the correct principal value integration. In our numerical analysis, we have taken $\epsilon = \epsilon_1 = \epsilon_2/2 = 0.001$. As stated before, the cutoff at $x = 0$ is imposed for the numerical calculation and has a small effect on the result. If, instead of imposing a cutoff on transverse momentum, Λ, we imposed a cutoff on the invariant mass [15], then the divergences at $x = 1$ would have been regulated by a nonzero photon mass [28]. The DVCS amplitude at $x = 1$ also receives a contribution from the single-particle sector of the Fock space [4,16,17,21], which we did not take into account. A detailed discussion about the cutoff scheme is provided in Appendix B.

All Fourier transforms have been performed by numerically calculating the Fourier sine and cosine transforms and then calculating the resultant by squaring them, adding and taking the square root, thereby yielding the Fourier spectrum (FS). The amplitude is divided by the normalization factor $\frac{e^4}{16\pi^3}$. In Fig. 2, we have shown the two-particle LFWFs of the electron as a function of x for different $k^\perp$. We have taken $m = 0.5$ MeV, $M = 0.51$ MeV, and $\lambda = 0.02$ MeV. The wave functions are similar for a slight change of parameter values; however, for $m < M$, there will be a node in $\psi_{-1/2+1}(x, k^\perp)$ at $m = xM$, which is seen in Fig. 2(c). The effect of the node is almost negligible for these parameter values.

In Fig. 3 we have shown the FS of the two-particle LFWFs given by Eqs. (3.7), for the same mass parameters as in Fig. 2. The FT has been taken with respect to x for fixed values of transverse momentum $k^\perp$. The wave functions $\eta_{1/2+1}$, $\eta_{-1/2+1}$, and $\eta_{1/2-1}$ are obtained as

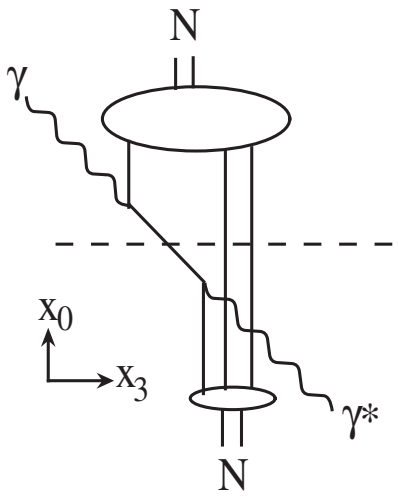

FIG. 1. The handbag diagram for the DVCS amplitude viewed in coordinate space. The position of the struck quark differs by x^- in the two wave functions (whereas $x^+ = x^\perp = 0$).

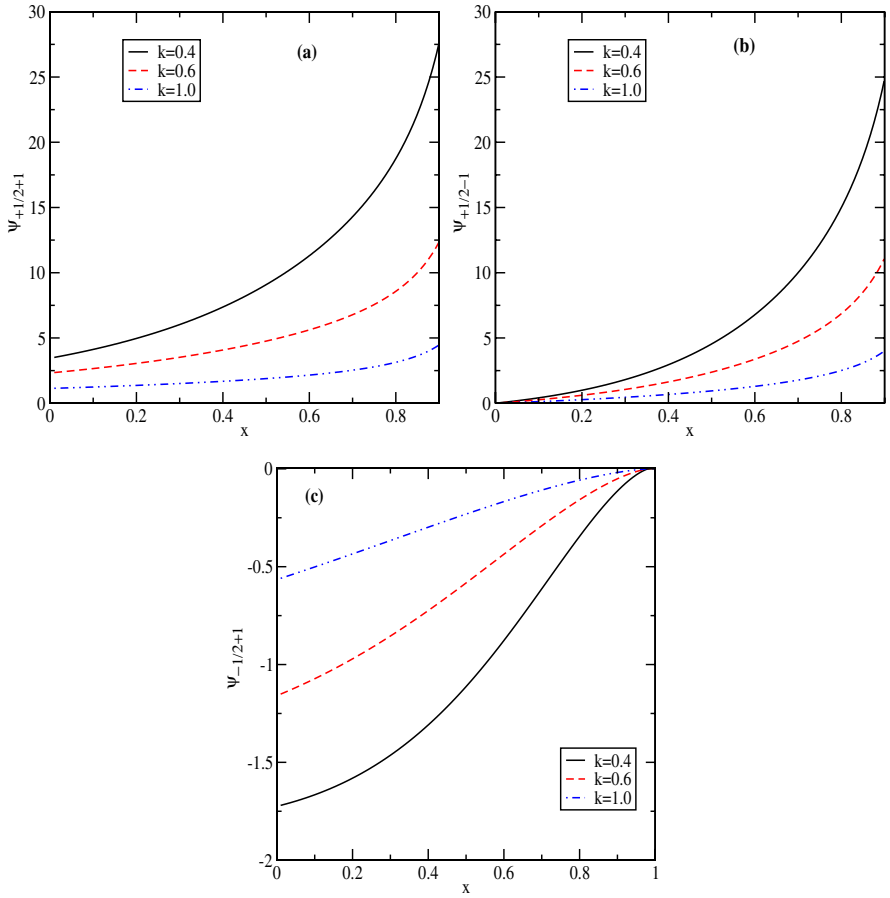

FIG. 2 (color online). Two-particle LFWFs of the electron vs x for $M = 0.51$ MeV, $m = 0.5$ MeV, $\lambda = 0.02$ MeV and fixed values of $|k^\perp| = k$ in units of MeV. In (b) and (c) we have divided the LFWFs by the factors $(k^1 + ik^2)$ and $(-k^1 + ik^2)$, respectively.

$$\eta^{\uparrow}_{1/2+1}(\sigma, k^\perp) = \frac{1}{2\pi(-k^1 + ik^2)} \times \int_0^1 dx e^{i\sigma(x-\hat{x}_k)} \psi^{\uparrow}_{1/2+1}(x, k^\perp),$$
$$\eta^{\uparrow}_{1/2-1}(\sigma, k^\perp) = \frac{1}{2\pi(k^1 + ik^2)} \times \int_0^1 dx e^{i\sigma(x-\hat{x}_k)} \psi^{\uparrow}_{1/2-1}(x, k^\perp),$$
$$\eta^{\uparrow}_{-1/2+1}(\sigma, k^\perp) = \frac{1}{2\pi} \int_0^1 dx e^{i\sigma(x-\hat{x}_k)} \psi^{\uparrow}_{-1/2+1}(x, k^\perp), \tag{4.2}$$

where $\hat{x}_k = \frac{\sqrt{m^2+k_\perp^2}}{\sum_i \sqrt{m_i^2+k_{\perp i}^2}}$ is the peak of the distribution—where all the constituents in the n-particle Fock state have equal rapidity.

All helicity components of the wave function show peaks at $\sigma = 0$; the height of the peak sharply increases as $k^\perp$ decreases and decays away from $\sigma = 0$. In Fig. 4, we have shown the complete Fourier transforms of the two-particle LFWF for $k = 0.2$ corresponding to the FS presented in Figs. 3(b) and 3(c) to illustrate the difference. Though the real and imaginary parts of the FT (i.e., the cosine and sine transforms, respectively) individually exhibit a diffraction pattern, in Fig. 4(a) they are just out of phase to produce any diffraction pattern in the FS. It is well known in the theory of the Fourier representation of signals [29] that the amplitude and phase play different roles and, in some cases, many of the important features of a signal are preserved only if the phase is retained.

The plots of the DVCS amplitude have been done by fixing $-t$ and varying both ζ and $\Delta_\perp$. In Fig. 5(a) we have shown the imaginary part of the helicity-flip DVCS amplitude M_{+-} as a function of ζ for different values of $-t$. $\mathrm{Im}[M_{+-}]$ is zero as $\zeta \to 0$, increases continually with ζ, and then falls down sharply at the end. It increases for higher t for the same ζ. Figure 5(b) shows the helicity-nonflip part of the corresponding amplitude $\mathrm{Im}[M_{++}]$ vs ζ. Unlike $\mathrm{Im}[M_{+-}]$, $\mathrm{Im}[M_{++}]$ is nonvanishing at $\zeta = 0$; it decreases for higher $-t$. The largest allowed value of ζ is given by Eq. (2.8) for fixed t. Figure 6(a) shows the plot of the real part of the helicity-flip DVCS amplitude for the same values of the parameters. $\mathrm{Re}[M_{+-}]$ is nonvanishing at $\zeta \to 0$. For small ζ, it is almost flat for a fixed $-t$ and

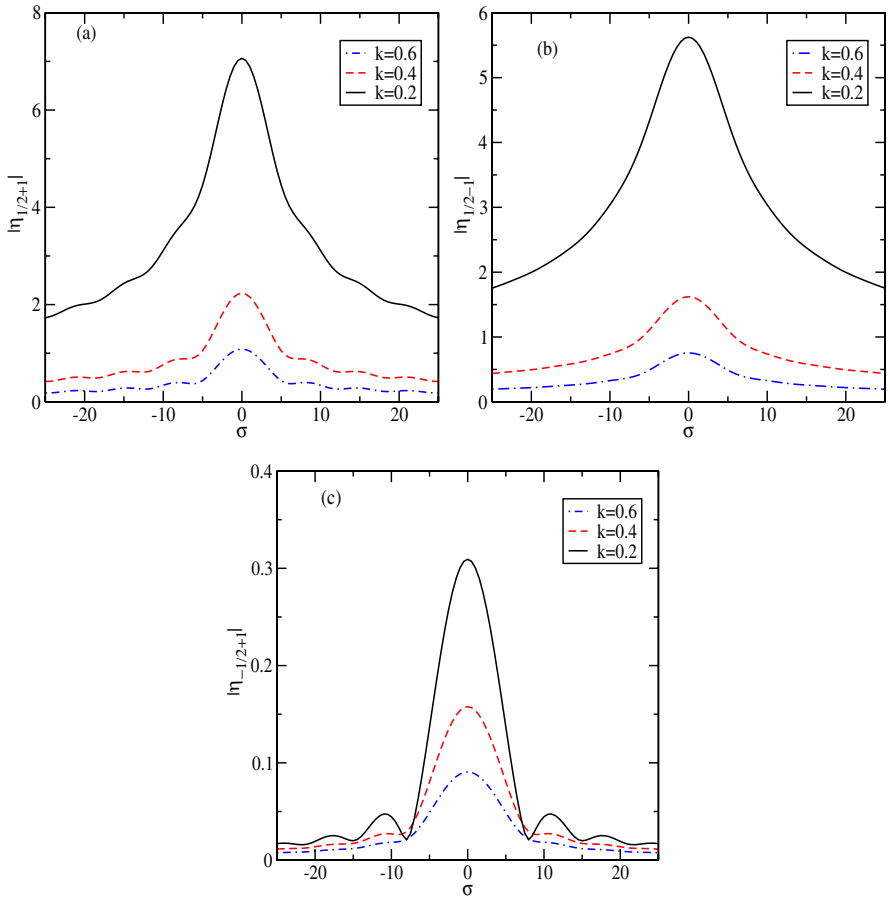

FIG. 3 (color online). Fourier spectrum of the two-particle LFWFs of the electron vs σ for $M = 0.51$ MeV, $m = 0.5$ MeV, $\lambda = 0.02$ MeV and fixed values of $|k^{\perp}| = k$ in MeV. In (b) and (c) we have divided the LFWFs by the factors $(k^1 + ik^2)$ and $(-k^1 + ik^2)$, respectively.

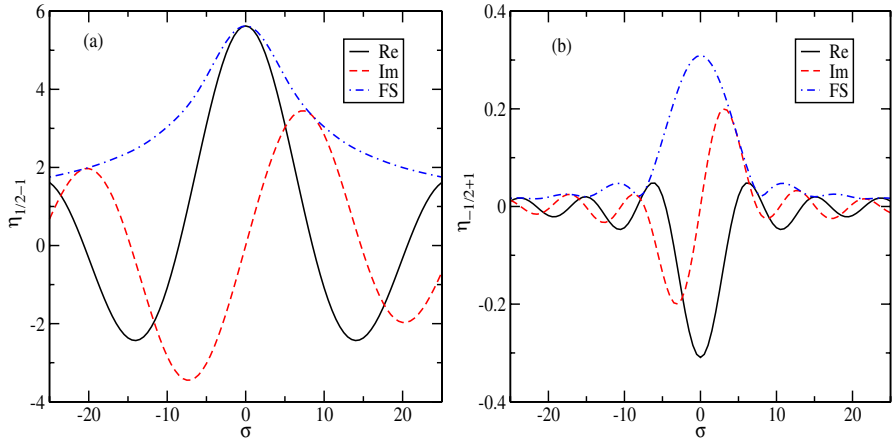

FIG. 4 (color online). FT of the two-particle LFWFs of the electron vs σ for $M = 0.51$ MeV, $m = 0.5$ MeV, $\lambda = 0.02$ MeV and fixed values of $|k^{\perp}| = k$ in MeV. Re and Im denote the real and imaginary parts of the FT, and FS denotes the Fourier spectrum presented in Figs. 3(b) and 3(c).

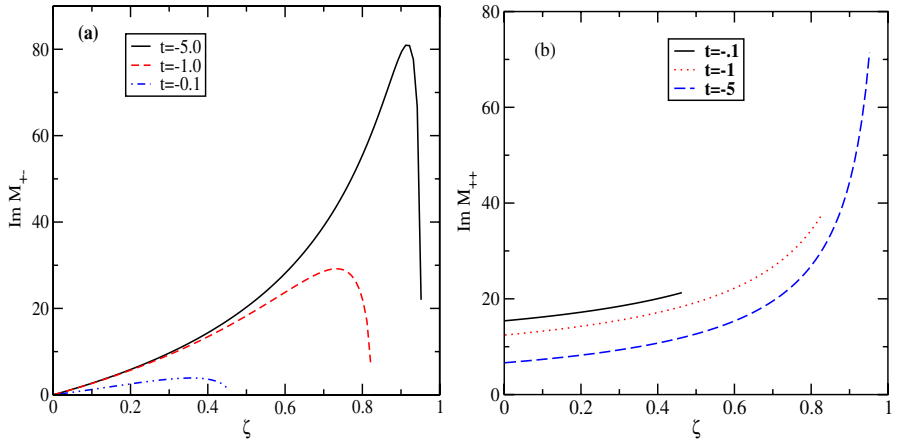

FIG. 5 (color online). Imaginary part of the DVCS amplitude for an electron vs ζ for different values of t: (a) helicity-flip part, (b) helicity-nonflip part. We have taken $M = 0.51$ MeV, $m = 0.5$ MeV, $\lambda = 0.02$ MeV. The parameter t is given in MeV.

then falls down at large ζ. Figure 6(b) shows the plot of the real part of the corresponding helicity-nonflip amplitude M_{++} vs ζ. It shows a different functional behavior as it increases both for small and large ζ.

Figure 7(a) shows the FS of the imaginary part of the helicity-flip amplitude vs σ for $M = 0.51$ MeV, $m = 0.5$ MeV, and $\lambda = 0.02$ MeV. The peak of the FS of $\mathrm{Im}[M_{+-}]$ (i.e.,$|\mathrm{Im}[A_{+-}]|$) increases with $|t|$. The increasing behavior of the helicity-flip amplitude $\gamma^* e^{\uparrow}(S_z^e = 1/2) \rightarrow \gamma e^{\downarrow}(S_z^e = -1/2)$ at small $|t|$ reflects the fact that one needs to transfer one unit of orbital angular momentum $\Delta L_z = \pm 1$ to the electron to conserve J_z. Note that the initial and final photons are taken to have transverse polarization. A similar behavior is expected for the $\gamma^* p^{\uparrow}(S_z^p = 1/2) \rightarrow \gamma p^{\downarrow}(S_z^p = -1/2)$ amplitude. The FS of $\mathrm{Im}[M_{+-}]$ does not show a diffraction pattern in σ. In Figs. 7(b) and 7(c) we have shown the FS of the imaginary part of the helicity-nonflip DVCS amplitude vs σ for the same parameter values. The helicity nonflip amplitude depends on the scale Λ. We have taken $\Lambda = Q$. Figure 7(b) shows the plot for $Q = 10$ MeV; Fig. 7(c) is for $Q = 50$ MeV. $\mathrm{Im}[A_{++}]$ shows a diffraction pattern; the peak becomes narrower as $|t|$ increases. In Fig. 8 we have shown the complete Fourier transform of the imaginary part of the DVCS amplitude corresponding to the FS presented in Fig. 7(a). It again shows that the real (cosine transform) and the imaginary (sine transform) of the Fourier transform individually show a diffraction pattern, but they are out of phase and thus the FS does not show the diffraction pattern.

The number of minima in the diffraction pattern increases with $|t|$ for fixed Q or, in other words, the first minima move in with an increase of $|t|$. For $Q = 50$ MeV, the behavior is the same; the number of minima are higher for higher t for the same σ range. The number and the positions of the minima are independent of Q. Only the magnitude of the peak changes with Q. Some of the plots of the FS of the DVCS amplitude show similarities with the

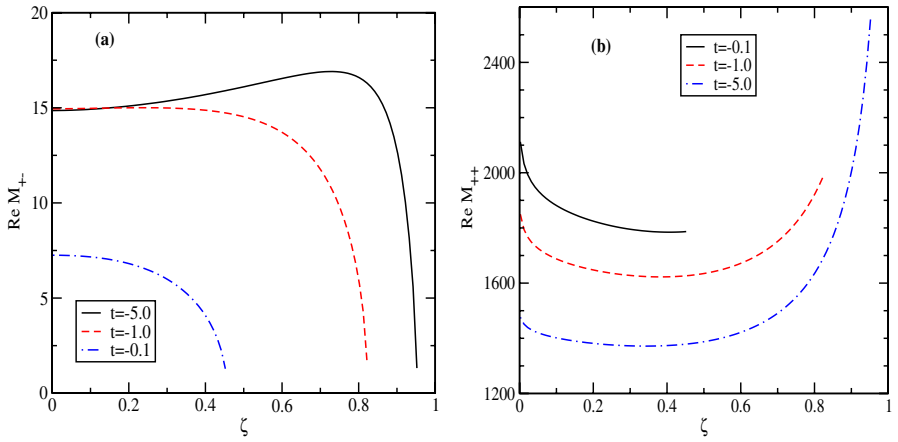

FIG. 6 (color online). Real part of the DVCS amplitude for an electron vs ζ for different values of t: (a) helicity-flip part, (b) helicity-nonflip part. We have taken $M = 0.51$ MeV, $m = 0.5$ MeV, $\lambda = 0.02$ MeV. The parameter t is given in MeV.

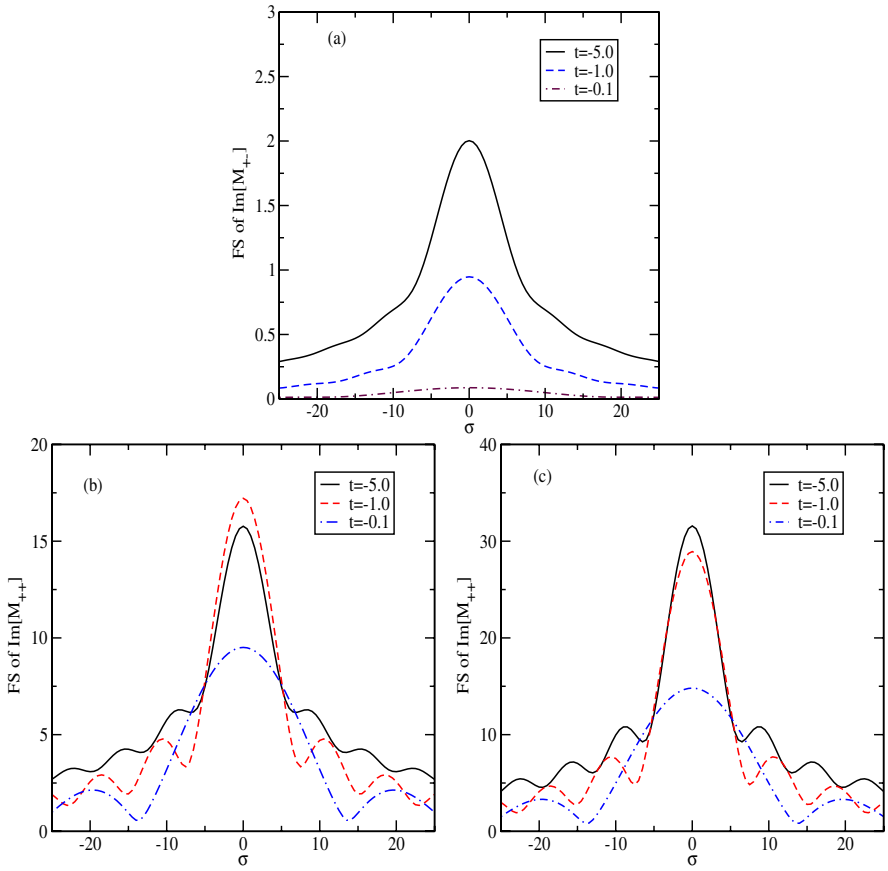

FIG. 7 (color online). Fourier spectrum of the imaginary part of the DVCS amplitude for an electron vs σ for different values of t: (a) when the electron helicity is flipped; (b) and (c) when the helicity is not flipped. In (b) $Q = 10$ MeV; in (c) $Q = 50$ MeV. The mass parameters are $M = 0.51$ MeV, $m = 0.5$ MeV, $\lambda = 0.02$ MeV. The parameter t is given in MeV.

FS of the LFWFs themselves. The generalized parton distributions are related to the form factors, and the form factors can be written as overlaps of LFWFs. In fact, for a meson in $1 + 1$-dimensional QCD, the form factor becomes an overlap of the LFWFs with different longitudinal momentum fractions, x [30], and the contribution is similar to the $2 \longrightarrow 2$ part of the DVCS amplitude.

Figure 9(a) shows the FS of the real part of the helicity-flip amplitude vs σ, where we chose the same values of the parameters, $M = 0.51$ MeV, $m = 0.5$ MeV, and $\lambda = 0.02$ MeV. The FS, i.e., $|\mathrm{Re}[A_{+-}]|$, shows a diffraction pattern in σ. With the increase of $-t$, the central peak increases and its width decreases. The helicity-flip part of the DVCS amplitude does not depend on Q.

The nonexistence of the diffraction pattern in the FS of the imaginary part of the helicity-flip amplitude in σ is due to its different behavior in ζ, as seen from Figs. 5 and 6. $\mathrm{Im}[M_{+-}]$ decreases smoothly as ζ decreases to vanish at $\zeta = 0$ which is distinctly different from all other amplitudes including $\mathrm{Re}[M_{+-}]$. All other amplitudes show some flatness or a plateau in ζ and their FS in σ space shows a diffraction pattern.

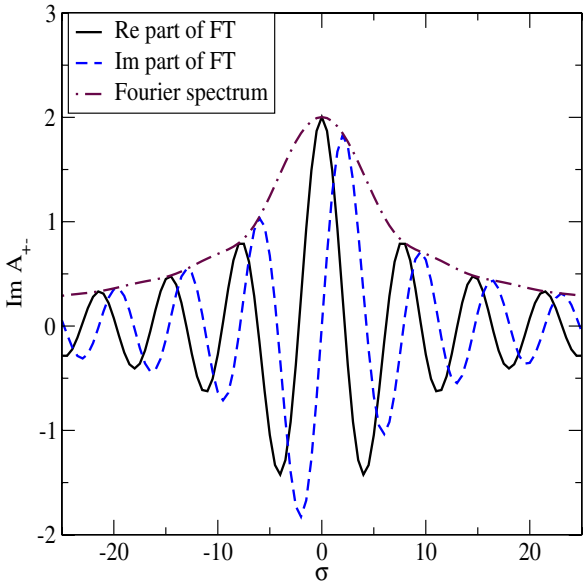

FIG. 8 (color online). FT of the imaginary part of the helicity-flip DVCS amplitude for an electron vs σ for $t = -5.0$. Re and Im denote the real and imaginary parts of the FT. The mass parameters are $M = 0.51$ MeV, $m = 0.5$ MeV, $\lambda = 0.02$ MeV.

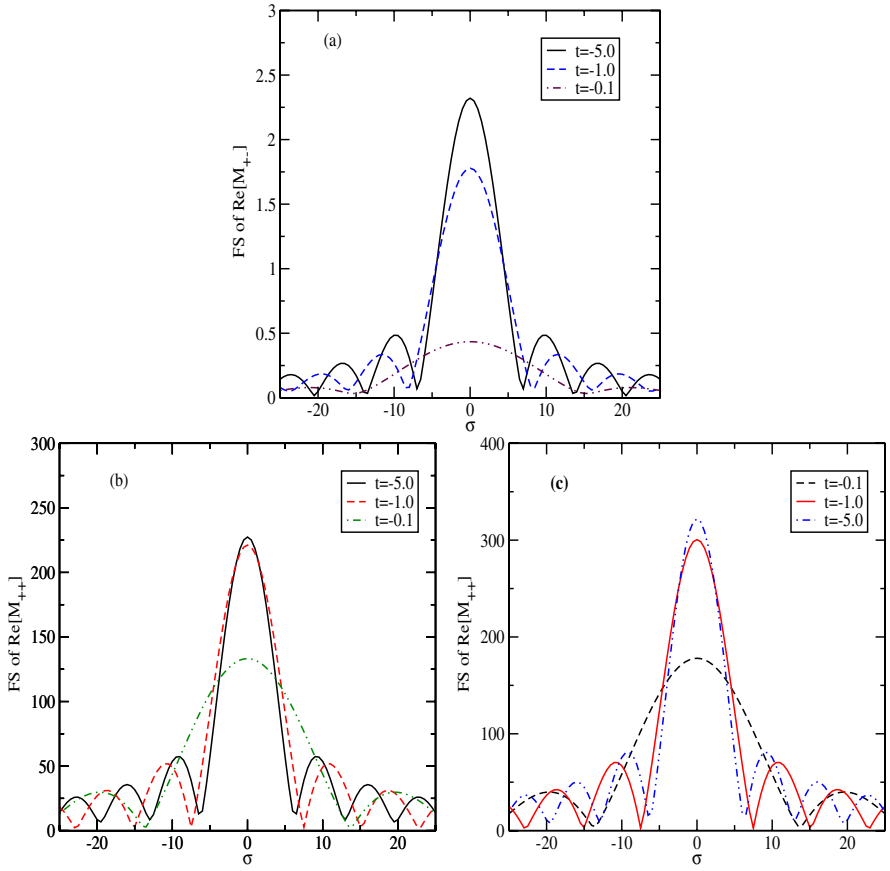

FIG. 9 (color online). Fourier spectrum of the real part of the DVCS amplitude for an electron vs σ for different values of t: (a) when the electron helicity is flipped; (b) and (c) when the helicity is not flipped. In (b) $Q = 10$ MeV; in (c) $Q = 50$ MeV. The mass parameters are $M = 0.51$ MeV, $m = 0.5$ MeV, $\lambda = 0.02$ MeV. The parameter t is given in MeV.

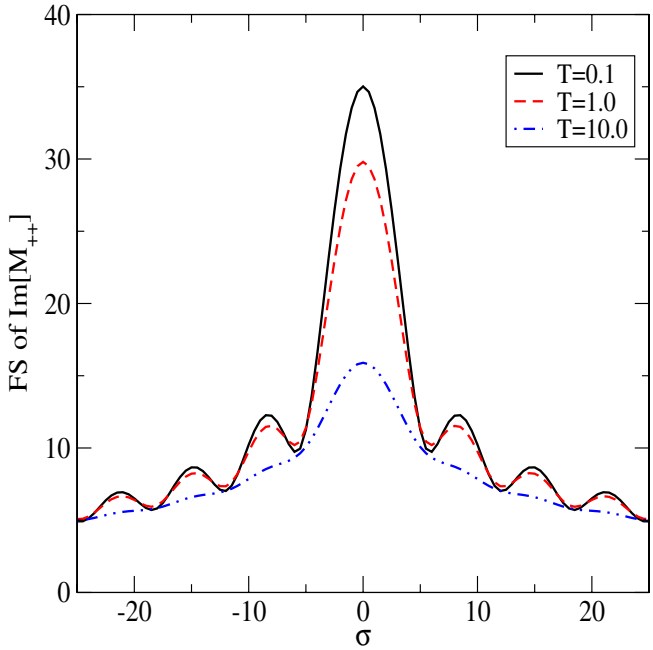

FIG. 10 (color online). Imaginary part of the helicity-nonflip DVCS amplitude for an electron vs σ for fixed T in MeV.

In Figs. 9(b) and 9(c), we have plotted the FS of the real part of the helicity-nonflip DVCS amplitude vs σ. One can see the diffraction pattern here as well. Figure 9(b) is for $Q = 10$ MeV and Fig. 9(c) is for $Q = 50$ MeV. As before, the qualitative behaviors of the diffraction pattern do not change with Q. For the same $|t|$, the number of minima and their positions are independent of Q for any fixed $|t|$; only the height changes with Q. For each Q, the peak at $\sigma = 0$ is sharper and higher as $|t|$ increases.

Instead of using the ζ and t variables, we can define another set of variables ζ and T, where T is defined as $T = (\frac{\Delta^\perp}{1-\zeta})^2$. The arguments of the final-state LFWF are then $x' = \frac{x-\zeta}{1-\zeta}$ and $k'^\perp = k^\perp - (1-x)\sqrt{T}$; in other words, the transverse momenta become decoupled from ζ. We can now take ζ and T as independent variables, and the GPDs as well as the DVCS amplitude can be expressed in terms of them. They are, however, connected through

$$t = -\frac{\zeta^2 M^2}{1-\zeta} - (1-\zeta)T. \tag{4.3}$$

This relation determines the range of allowed values of ζ and T, such that $t \ll Q^2$. In practice, ζ can never become

very close to 1. The ζ dependence of the DVCS amplitude now comes purely from x' for fixed T. Figure 10 shows a plot of the imaginary part of the helicity-nonflip amplitude for fixed T vs σ. For very small σ, the slope of the σ distribution is given by

$$\frac{d}{d\sigma}\,\mathrm{Im}A_{++} \to \int_{\epsilon}^{1-\epsilon} dx x(F^{22}_{++}(x,x,T) + F^{31}_{++}(x,x,T)). \tag{4.4}$$

Thus the slope and therefore the width of the σ distribution depend on the second moment of the GPDs at $x = \zeta$.

V. SIMULATED BOUND STATES

For the dressed electron state, the real part of the DVCS amplitude depends on the cutoffs at $x = 0$ and $x = 1$. We have chosen the cutoff scheme discussed earlier. The cutoff at $x = 0$ is taken for the numerical calculation and its effect on the result is small. However, starting from this QED pointlike model where the electron fluctuates to spin-half plus spin-one constituents, one can construct LFWFs for the hadrons. In the two- and three-particle LFWFs for the electron, the bound-state mass M appears in the energy denominators. A differentiation of the QED LFWFs with respect to M^2 improves the convergence at the end points, $x = 0$, 1, as well as at high $k_\perp^2$, thus simulating a bound-state valence wave function. Differentiating once with respect to M^2 will generate a mesonlike behavior of the LFWF. Thus we write the hadron two-particle LFWFs as

$$\tilde{\psi}_{s_1 s_2}(x, k_\perp) = M^2 \frac{\partial}{\partial M^2}\psi_{s_1 s_2}(x, k_\perp), \tag{5.1}$$

where $\psi_{s_1 s_2}(x, k_\perp)$ are the electron LFWFs. Taking the Fourier transform in $k_\perp$ also, we can write the wave functions in σ and the transverse impact parameter $b_\perp$ as

$$\chi_{s_1 s_2}(\sigma, b_\perp) = \frac{1}{(2\pi)^3}\int_0^1 dx \int d^2k_\perp e^{i\sigma(x-\hat{x}_k)} e^{ik_\perp \cdot b_\perp} \times \tilde{\psi}_{s_1 s_2}(x, k_\perp), \tag{5.2}$$

where the peak of the distribution appears at $\hat{x}_k = \frac{\sqrt{m^2+k_\perp^2}}{\sum_i \sqrt{m_i^2+k_{\perp i}^2}}$. Writing $k_\perp \cdot b_\perp = kb\cos\theta$, where $b = |b_\perp|$ and $k = |k_\perp|$, and performing the integration over θ, we obtain

$$\chi_{s_1 s_2}(\sigma, b_\perp) = \frac{1}{(2\pi)^3}\int_0^1 dx \int kdk e^{i\sigma(x-\hat{x}_k)}(2\pi)J_0(bk) \times \tilde{\psi}_{s_1 s_2}(x, k_\perp), \tag{5.3}$$

where $J_0(bk)$ is the Bessel function. For the wave functions $\chi_{1/2\pm1}$ we have the explicit momentum components $(k_1 \pm ik_2)$ present in the numerators. We use

$$\begin{aligned}\int d^2k_\perp (k_1 \pm ik_2) e^{ik_\perp\cdot b_\perp} &= (-i)\int d^2k_\perp \left(\frac{\partial}{\partial b_1} \pm i\frac{\partial}{\partial b_2}\right) e^{ik_\perp\cdot b_\perp} = (-i)\int kdkd\theta \frac{k(b_1 \pm ib_2)}{b}\frac{\partial}{\partial(kb)} e^{ikb\cos\theta} \\ &= (-i)\int k^2dk\frac{(b_1 \pm ib_2)}{b}\frac{\partial}{\partial(kb)}(2\pi)J_0(kb) = 2\pi i\int k^2dk\frac{(b_1 \pm ib_2)}{b}J_1(kb).\end{aligned} \tag{5.4}$$

For the plot of the wave functions, we set $b_2 = 0$ in the above expression,

$$\begin{aligned}\chi_{+1/2+1}(\sigma, b) &= \frac{e}{(2\pi)^2}\sqrt{2}M^2 i\int dx\int k^2dk\frac{x(1-x)^{1/2}J_1(kb)e^{i\sigma(x-\hat{x}_k)}}{(M^2x(1-x)-k^2-m^2(1-x)-\lambda^2x)^2}, \\ \chi_{+1/2-1}(\sigma, b) &= \frac{e}{(2\pi)^2}\sqrt{2}M^2 i\int dx\int k^2dk\frac{x^2(1-x)^{1/2}J_1(kb)e^{i\sigma(x-\hat{x}_k)}}{(M^2x(1-x)-k^2-m^2(1-x)-\lambda^2x)^2}, \\ \chi_{-1/2+1}(\sigma, b) &= \frac{e}{(2\pi)^2}\sqrt{2}M^2 \int dx\int kdk\frac{x^2(1-x)^{3/2}J_0(kb)e^{i\sigma(x-\hat{x}_k)}}{(M^2x(1-x)-k^2-m^2(1-x)-\lambda^2x)^2}.\end{aligned} \tag{5.5}$$

For computational purpose, we use

$$J_n(kb) = \frac{1}{\pi}\int_0^\pi d\theta\cos(n\theta - kb\sin\theta). \tag{5.6}$$

This procedure does not provide an actual model for a ''meson'' wave function since the two constituents have spin-half and spin-one. However, if we differentiate once more we can simulate the falloff at short distances which matches the falloff wave function of a baryon, in the sense that the form factor $F_1(Q^2)$ computed from the Drell-Yan-West formula will fall off like $\frac{1}{Q^4}$. In this case, we obtain a quark plus spin-one diquark model of a baryon. Convolution of these wave functions in the same way as we have done for the dressed electron wave functions will simulate the corresponding DVCS amplitudes for bound-state hadrons. Note that the differentiation of the single-particle LFWF will give a vanishing result and, as a result, the $3 \to 1$ contribution to the DVCS amplitude vanishes in this model. The resulting $\gamma^* p \to \gamma p$ DVCS amplitude has both real [2] and imaginary parts [3].

If we consider a dressed electron, the imaginary part from the pole at $x = \zeta$ survives because of the numerator $\frac{1}{x-\zeta}$ factor in the electron's LFWF. This numerator behavior reflects the spin-1 nature of the constituent boson. The $x - \zeta \to 0$ singularity is shielded when we differentiate the final-state $n = 2$ and $n = 3$ LFWFs with respect to M^2 and, as a result, the imaginary part of the amplitude vanishes in this model. We thus have constructed a model where the DVCS amplitude is purely real. However, the forward virtual Compton amplitude $\gamma^* p \to \gamma^* p$ (whose imaginary part gives the structure function) does not have this property. The pole at $x = \zeta$ is not shielded since the initial and final $n = 2$ LFWFs are functions of x. It is worthwhile to point out that, in general, the LFWFs for a hadron may be nonvanishing at the end points [31], and recent measurements of single-spin asymmetries suggest that the GPDs are nonvanishing at $x = \zeta$ [32]. A more realistic estimate would require nonvalence Fock states [33]. An equivalent but easier way to construct the hadronic model is to differentiate the DVCS amplitudes with respect to the invariant mass squared (M^2) of the initial and final bound states. Thus one can calculate the quantity $M_F^2 \frac{d}{dM_F^2} M_I^2 \frac{d}{dM_I^2} A_{ij}(M_I, M_F)$, where M_I, M_F are the initial and final bound-state masses.

For numerical computation we use the discrete (in the sense that the denominator is finite) version of the differentiation:

$$M^2 \frac{dA}{dM^2} = \bar{M}^2 \frac{A(M_1^2) - A(M_2^2)}{\delta M^2}, \tag{5.7}$$

where $\bar{M}^2 = (M_1^2 + M_2^2)/2$ and $\delta M^2 = (M_1^2 - M_2^2)$. Then we have

$$\begin{aligned} &M_F^2 \frac{d}{dM_F^2} M_I^2 \frac{d}{dM_I^2} A_{ij}(M_I, M_F) \\ &\quad = \frac{\bar{M}_I^2 \bar{M}_F^2}{\delta M_I^2 \delta M_F^2} [A_{ij}(M_{I1}, M_{F1}) - A_{ij}(M_{I1}, M_{F2}) \\ &\qquad - A_{ij}(M_{I2}, M_{F1}) + A_{ij}(M_{I2}, M_{F2})]; \end{aligned} \tag{5.8}$$

$A_{ij}(M_I, M_F)$ is the DVCS amplitude for an electron. The differentiation with respect to M_F^2 of the amplitudes (helicity flip and nonflip) brings in an extra factor of $x - \zeta$ and thus the imaginary parts of the DVCS amplitudes vanish in

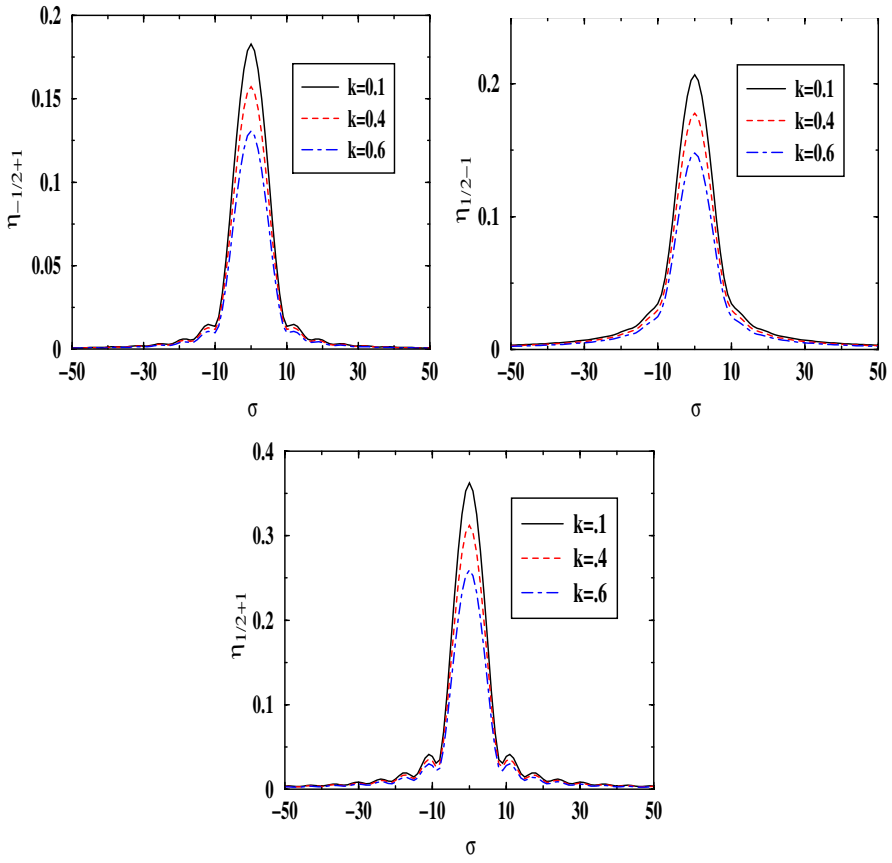

FIG. 11 (color online). Fourier spectrum of the LFWFs of the simulated hadron model vs σ for $M = 0.5$ MeV, $m = \lambda = 1.0$ MeV and fixed values of $|k^\perp| = k$ in MeV. We have divided the LFWFs by the normalization constant. In (b) and (c) we have divided by the factors $(k^1 + ik^2)$ and $(-k^1 + ik^2)$, respectively, as well.

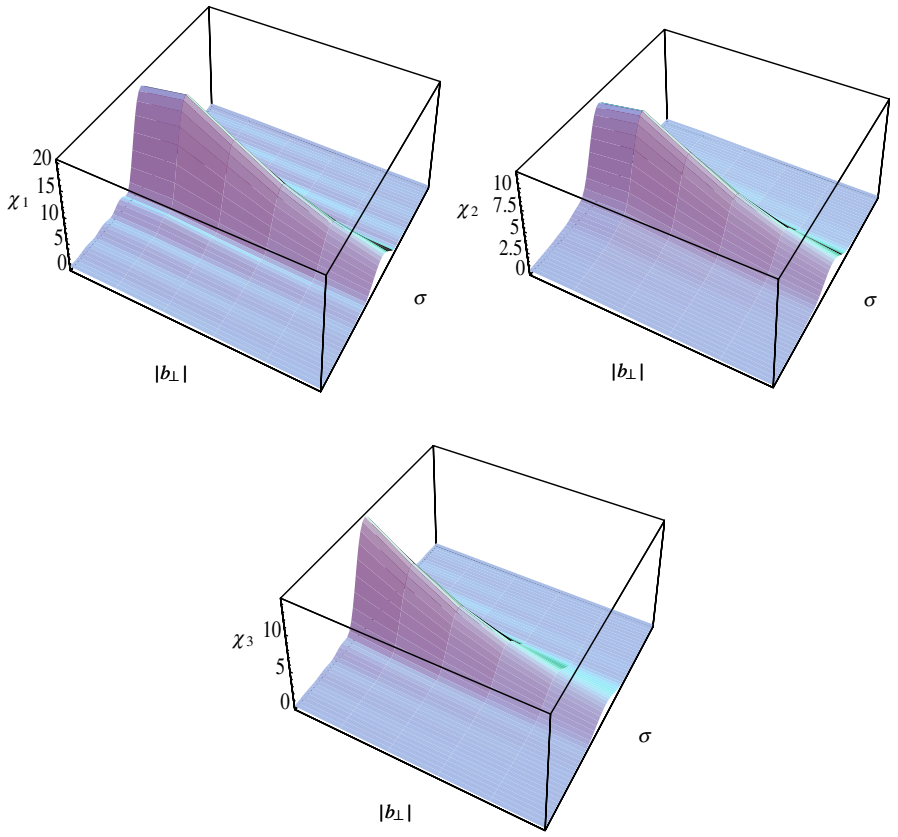

FIG. 12 (color online). Fourier spectrum of the LFWFs of the simulated hadron model plotted in $\sigma, |b_\perp|$ space for $M = 150$ MeV, $m = \lambda = 300$ MeV. χ_1, χ_2, and χ_3 are $|\chi_{1/2+1}|$, $|\chi_{1/2-1}|$, and $|\chi_{-1/2+1}|$, respectively. In the plots $|b_\perp|$ runs from 0.001 to 0.01 MeV^{-1} and σ runs from -25 to $+25$.

this model, as discussed before. The real parts of the DVCS amplitudes survive and show diffraction patterns. We take $M_{I1}, M_{F1} = 150 + 1.0$ and $M_{I2}, M_{F2} = 150 - 1.0$ and the fixed parameters $M = 150$, $m = \lambda = 300$ MeV. In Figs. 11 and 12 we have shown the FS of the two-particle LFWFs for this model. The parameter values are scaled in Fig. 11, but the qualitative behaviors are the same. Since the wave function now vanishes at $x = 0$, 1, the FS is localized, and it decays sharply beyond $|\sigma| = 10$. The peak decreases more sharply for higher $k_\perp$ or lower $|b_\perp|$. In Figs. 13(a) and 13(b) we have shown the helicity-flip DVCS amplitude for the hadron model as a function of ζ

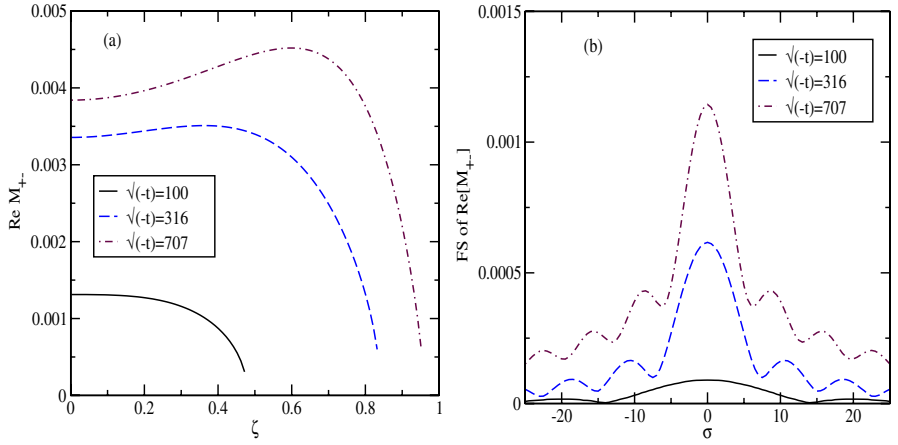

FIG. 13 (color online). Real part of the DVCS amplitude for the simulated hadron state. The parameters are $M = 150$, $m = \lambda = 300$ MeV. (a) Helicity-flip amplitude vs ζ; (b) Fourier spectrum of the same vs σ. The parameter t is in MeV^2.

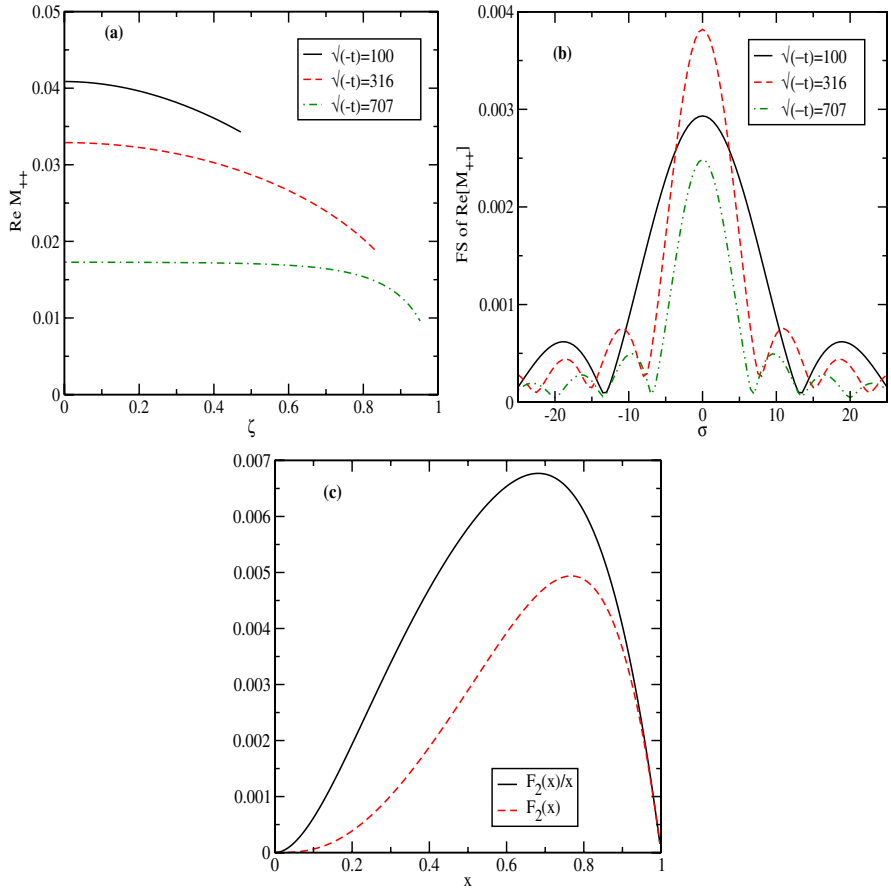

FIG. 14 (color online). Real part of the DVCS amplitude for the simulated hadron bound state. The parameters are $M = 150$, $m = \lambda = 300$ MeV. (a) Helicity-nonflip amplitude vs ζ; (b) Fourier spectrum of the same vs σ; (c) structure function vs x. The parameter t is in MeV^2.

and its FS as a function of σ, respectively. In Figs. 14(a) and 14(b) we have shown the real part of the helicity-nonflip amplitudes of the same model as a function of ζ and its FS as a function of σ, respectively. Notice that the helicity-nonflip part of the amplitude no longer depends on the scale. The amplitude decreases as ζ increases, in contrast to the behavior for the electron. The FS of both the helicity-flip and nonflip DVCS amplitudes shows a diffraction pattern in σ. Figure 14(c) illustrates the structure function $F_2(x)$ for this model as a function of x.

An optical analog

We propose an optics analog of the behavior of the FT of DVCS amplitude in σ. The similarity of optics and quantum fields on the light cone was first explored long ago by Sudarshan, Simon, and Mukunda. They established the similarity of paraxial-wave optics and light-cone dynamics of scalar [34] and Maxwell equations [35]. In our case, we are effectively looking at the interference between the initial and final waves of the scattered proton. The final-state proton wave function is modified relative to the incident proton wave function because of the momentum transferred to the quark in the hard Compton scattering. The change in quark momentum along the longitudinal direction can be Fourier transformed to a shift in the light-front position of the struck quark; thus one can simulate a change in the quark's longitudinal LF coordinate by an amount $\sigma = \frac{1}{2} b^- P^+$. This is analogous to diffractive scattering of a wave in optics where σ plays the role of the physical size of the scattering center in a one-dimensional system. We are using t to register the change in the transverse momentum of the quark in the scattering. The position of the first minimum moves in with increasing $|t|$.

Notice that the integrals over x and ζ are of finite range. More importantly, the upper limit of the ζ integral is $\zeta_{\max}$, which in turn is determined by the value of $-t$. The finiteness of the slit width is a *necessary* condition for the occurrence of a diffraction pattern in optics. Thus, when the integration is performed over the range 0 to $\zeta_{\max}$, the finite range acts as a slit of finite width and provides a necessary condition for the occurrence of a diffraction pattern in the Fourier transform of the DVCS amplitude.

When a diffraction pattern is produced, in analogy with single slit diffraction, we expect the position of the first minimum to be inversely proportional to $\zeta_{\max}$. Since $\zeta_{\max}$

TABLE I. Positions of minima in the diffraction pattern for different $-t$ for the simulated hadron model DVCS amplitudes.

	σ (MeV^{-1})		
$\sqrt{-t}$ (MeV)	1st min	2nd min	3rd min
100	13.5		
141	10.5	21.0	
223	8.5	17.0	25.5
264	8.0	16.0	24.0
316	7.5	15.0	22.5
707	7.0	13.5	20.0

increases with $-t$, we expect the position of the first minimum to move to a smaller value of σ, in analogy with optical diffraction. In the case of the Fourier spectrum of DVCS on the quantum fluctuations of a lepton target in QED, and also in the corresponding hadronic model, one sees that the diffractive patterns in σ sharpen and the position of the first minimum moves in with increasing momentum transfer. Thus the invariant longitudinal size of the parton distribution becomes longer and the shape of the conjugate light-cone momentum distribution becomes narrower with increasing $|t|$.

From Table I, we can see that, for a fixed $(-t)$, higher minima appear at positions which are integral multiples of the lowest minima. This is consistent with the single slit diffraction law for nth minima: $\sin\theta_n = n\lambda/w$, where λ is the wavelength of the light and w is the slit width. Here σ plays the role of $\sin\theta_n$ [for large separation (L) between the slit and the detector in a single slit experiment, one can write $\sin\theta_n \approx \frac{\sigma_n}{L}$] and the ratio λ/w is determined by the value of $-t$. Positions of the minima do not depend on the helicity. The minima appear at the same places for both helicity-flip and nonflip processes.

We also observe a relation between the invariant momentum transfer squared $-t$ and the distribution in σ: the first minimum in a diffraction pattern is determined by

$$\sin\theta_1 = \frac{\sigma_1}{\sqrt{L^2 + \sigma_1^2}} = \frac{\lambda}{w}, \tag{5.9}$$

where σ_1 is the position of the first minimum measured from the center of the diffraction pattern. Introducing another parameter t_0, with $-t > -t_0$, we write the right-hand side, i.e., the ratio $\frac{\lambda}{w}$, as $\frac{1}{\log(-t+t_0)}$ where we have chosen $-t_0 = 2 \times 10^4$ MeV^2. Once t_0 is fixed, the other parameter L can be found; $\sigma_1 = 8.5$ MeV^{-1} for $-t = 5 \times 10^4$ MeV^2 gives

$$\frac{8.5}{\sqrt{L^2 + 8.5^2}} = \frac{1}{\log(3 \times 10^4)} = 0.2234$$

which gives $L^2 \approx 1376$ MeV^{-2}. Using this value of L, we can compare with the other data.

TABLE II. Comparison of our proposed formula with the data. $\sqrt{-t}$ is in MeV and the lengths are in MeV^{-1}.

$\sqrt{-t}$	σ_1	$\frac{\sigma_1}{\sqrt{L^2+\sigma_1^2}}$	$\frac{1}{\log(-t+t_0)}$
264	8.0	0.211	0.213
316	7.5	0.198	0.204
707	7.0	0.185	0.176

Table II shows that our parametrization of $\frac{\lambda}{w}$ in terms of $-t$ is quite accurate.

If one Fourier transforms the change in transverse momentum $\Delta_\perp$ to impact space $b_\perp$ [6,7], then one would have the analog of a three-dimensional scattering center. In this sense, studying the FT of the DVCS is very much like studying the Lorentz-invariant optics of the proton. In our analysis we have computed DVCS on an electron at $O(\alpha)$ and its FT. Thus we have obtained the diffractive optics of the quantum fluctuations of an electron.

It is interesting to recall that the scattering amplitude corresponding to an absorptive (i.e., negative imaginary) potential which is confined to a sphere of finite radius exhibits a diffraction pattern. For a classic treatment, see R. J. Glauber's lectures [36]. For another example of diffraction patterns in the angular distribution of elastic proton-nucleus scattering using a multiple-scattering approach, see Ref. [37]. It is worthwhile to remember that in these examples the optical potential is complex. In our case, we observe diffraction patterns when we perform Fourier transforms of real functions.

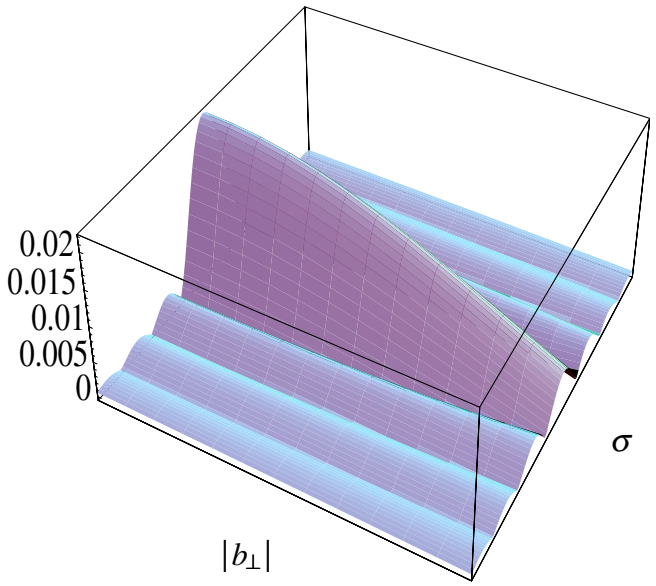

FIG. 15 (color online). The ground state $(L = 0, k = 1)$ of the two-parton holographic light-front wave function in 3D space. We have taken $\Lambda_{\rm QCD} = 0.32$ GeV. Here $|b_\perp|$ runs from 0.001 to 6.0 GeV^{-1} and σ from -25 to 25.

VI. LFWF FOR MESONS IN HOLOGRAPHIC QCD AND THE DVCS AMPLITUDE

The normalized holographic QCD LFWF for the meson $(q\bar{q})$ from AdS/CFT derived in Ref. [24] is

$$\Psi_{L,k}(x, b_\perp) = B_{L,k}\sqrt{x(1-x)}J_L(\xi\beta_{L,k}\Lambda_{\rm QCD}), \qquad (6.1)$$

where $B_{L,k} = \Lambda_{\rm QCD}[(-1)^L \pi J_{1+L}(\beta_{L,k})J_{1-L}(\beta_{L,k})]^{-1/2}$, $\xi = \sqrt{x(1-x)}|b_\perp|$, and $\beta_{L,k}$ is the kth zero of the Bessel function J_L. For the ground state $L = 0$, $k = 1$ and we have

$$\phi(x, b_\perp) = \Psi_{0,1}(x, b_\perp) = \Lambda_{\rm QCD}\sqrt{x(1-x)}\frac{J_0(\xi\beta_{0,1}\Lambda_{\rm QCD})}{\sqrt{\pi}J_1(\beta_{0,1})}. \qquad (6.2)$$

The corresponding momentum space LFWF is [24]

$$\psi(x, \kappa_\perp) = \sqrt{4\pi^2}\int d^2b_{1\perp}e^{-ib_{1\perp}\cdot\kappa_\perp}\phi(x, b_{1\perp}). \qquad (6.3)$$

In Fig. 15, we have plotted the two-parton bound-state holographic LFWF from the AdS/CFT correspondence in 3D coordinate space after taking the FT of Eq. (6.2) with respect to x. The ADS/CFT correspondence gives only the wave function for the $q\bar{q}$ sector. So, when we consider the DVCS amplitude with this wave function, we can have contribution only from the $2 \to 2$ process. Then the DVCS amplitude can be written as

$$M(\Delta_\perp, \zeta) = -e_q^2\sum_{\sigma_1,\sigma_2}\int_\zeta^1 dx\left[\frac{1}{x-\zeta+i\epsilon}+\frac{1}{x-i\epsilon}\right]\int d^2\kappa_\perp\left[\psi^*_{\sigma_1,\sigma_2}\left(\frac{x-\zeta}{1-\zeta}, \kappa_\perp - \frac{1-x}{1-\zeta}\Delta_\perp\right)\psi_{\sigma_1,\sigma_2}(x, \kappa_\perp) + \psi^*_{\sigma_1,\sigma_2}\left(\frac{1-x}{1-\zeta}, \kappa_\perp + \frac{1-x}{1-\zeta}\Delta_\perp\right)\psi_{\sigma_1,\sigma_2}(1-x, \kappa_\perp)\right]. \qquad (6.4)$$

The transverse Fourier transform of the DVCS amplitude gives the DVCS amplitude in the transverse impact parameter space $b_\perp$,

$$\tilde{A}(b_\perp, \zeta) = \frac{1}{(2\pi)^2}\int d^2\Delta_\perp e^{ib_\perp\cdot\Delta_\perp}M(\Delta_\perp, \zeta). \qquad (6.5)$$

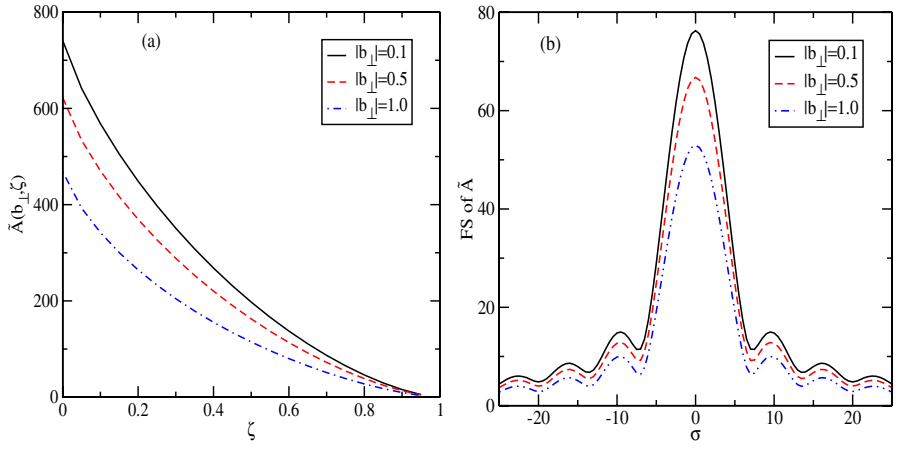

FIG. 16 (color online). (a) The DVCS amplitude vs ζ and (b) the Fourier spectrum of the DVCS amplitude in the σ space using the light-front wave function for mesons obtained from holographic QCD [24]. We have taken $\Lambda_{\rm QCD} = 0.32$ GeV. Plots are in units of e_q^2. $b^\perp$ is given in units of GeV^{-1}.

Then

$$\tilde{A}(b_\perp, \zeta) = (2\pi)^4 \int dx F(x,\zeta) \frac{1-\zeta}{1-x} \times \Big[\phi^*\Big(\frac{x-\zeta}{1-\zeta}, \frac{1-\zeta}{1-x} b_\perp\Big) \phi\Big(x, \frac{1-\zeta}{1-x} b_\perp\Big) + \phi^*\Big(\frac{1-x}{1-\zeta}, -\frac{1-\zeta}{1-x} b_\perp\Big) \times \phi\Big(1-x, -\frac{1-\zeta}{1-x} b_\perp\Big)\Big], \tag{6.6}$$

where $F(x,\zeta) = -e_q^2(\frac{1}{x} + \frac{1}{x-\zeta})$. Taking the FT of this DVCS amplitude with respect to ζ, we obtain the amplitude in the three-dimensional impact parameter space σ, $b_\perp$. Substituting the wave functions given in Eq. (6.2), we obtain

$$A(\sigma, b_\perp) = \frac{1}{2\pi} \int d\zeta e^{i\sigma\zeta} \tilde{A}(b_\perp, \zeta) = 2(2\pi)^4 \frac{\Lambda_{QCD}^2}{2\pi^2 J_1(\beta_{0,1})^2} \int_0^1 d\zeta e^{i\sigma\zeta} \times \int_\zeta^1 dx F(x,\zeta) \sqrt{x(x-\zeta)} [J_0(X_1) J_0(X_2)], \tag{6.7}$$

where

$$X_1 = \sqrt{x(1-x)} \frac{1-\zeta}{1-x} |b_\perp| \beta_{0,1} \Lambda_{\rm QCD},$$

$$X_2 = \sqrt{(1-x)(x-\zeta)} \frac{1}{1-x} |b_\perp| \beta_{0,1} \Lambda_{\rm QCD}.$$

In Fig. 16 we show the FS of the DVCS amplitude in σ space for different fixed values of $|b_\perp|$. Again we see the diffraction pattern in the σ space.

VII. SUMMARY AND CONCLUSIONS

The deeply virtual Compton scattering process $\gamma^* p \to \gamma p$ provides a direct window into the hadron substructure which goes well beyond inclusive measurements. The DVCS amplitude factorizes into the convolution of a hard perturbative amplitude, corresponding to Compton scattering on a quark current, with the initial- and final-state light-front wave functions of the target hadron. The LFWFs provide a general frame-independent representation of relativistic composite hadrons, and they are universal and process independent.

In this paper, we have shown that the Fourier transform of the DVCS amplitude with respect to the skewness variable ζ gives information of the proton structure in longitudinal impact parameter space $\sigma = \frac{1}{2} P^+ b^-$.

As an illustration of our general framework, we have worked with a simple relativistic spin $1/2$ system, namely, the quantum fluctuations of a lepton at one loop in QED. The different Fock components of the LFWFs in this case can be obtained from perturbation theory. Our calculation is exact to $O(\alpha)$. This one-loop model provides a transparent basis for understanding the structure of more general bound-state systems. By differentiating the wave functions for the electron with respect to the square of the bound-state mass M^2, we have simulated bound-state valence wave functions.

We have noted that there are two different types of overlaps contributing to DVCS when ζ is nonzero, namely, a parton number conserving diagonal $2 \to 2$ overlap and a $3 \to 1$ overlap when an electron-positron pair of the initial state is annihilated. In fact, both these contributions are necessary in order to obtain ζ independent form factors by taking the x moment of the GPDs. This invariance is due to the Lorentz frame independence of the light-front Fock representations of spacelike local operator matrix elements, and it reflects the underlying connections of Fock states with different parton numbers implied by the equation of motion. The Fourier transform of the amplitude with respect to ζ involves both types of contributions in different kinematical regions.

We have introduced the light-cone longitudinal distance $\sigma = P^+ b^-/2$ and have shown the σ dependence of the real and imaginary parts of the DVCS amplitude. The DVCS amplitude in σ space represents an interference of the initial- and final-state LFWFs. We have also shown the σ dependence of the LFWFs themselves.

We have exhibited the light-front coordinate space structure of our model wave functions by performing the Fourier transform in the longitudinal and transverse momentum space. The wave functions exhibit diffraction patterns in the longitudinal coordinate space. We have presented the FS of the real part of the DVCS amplitude as well as the structure function in the models. The corresponding imaginary part of the model DVCS amplitudes vanishes.

Very recently, valence parton bound-state holographic LFWFs from the AdS/CFT correspondence have been given [24]. We have presented these wave functions for the meson in full three-dimensional light-front coordinate space. We have also calculated the real part of the DVCS amplitude in the holographic model in light-front longitudinal space for specific choices of the impact parameter ($b_\perp$). Again one observes diffraction patterns. Note that the imaginary part of the DVCS amplitudes vanishes also in this model.

Our analysis is the first to examine the longitudinal light-cone coordinate $\sigma = b^- P^+/2$ dependence of LFWFs and DVCS amplitudes. Our results for the DVCS amplitude in σ are analogous to diffractive scattering of a wave in optics where the σ distribution senses the size of the one-dimensional scattering center. Thus studying DVCS $\gamma^* p \to \gamma p$ in light-front longitudinal coordinate space is very much like studying the Lorentz-invariant optics of the proton.

ACKNOWLEDGMENTS

This work was supported, in part, by the US Department of Energy Grant No. DE-AC02-76SF00515 and No. DE-FG02-87ER40371. This work was performed, in part, under the auspices of the US Department of Energy by the University of California, Lawrence Livermore National Laboratory under Contract No. W-7405-Eng-48. This work was also supported, in part, by the Indo-US Collaboration project jointly funded by the U.S. National Science Foundation (NSF) (INT0137066) and the Department of Science and Technology, India (DST/INT/US (NSF-RP075)/2001). The work of D. C. was supported, in part, by US Department of Energy under Grant No. DE-FG02-97ER-41029. We thank Professor Guy de Teramond for helpful conversations.

APPENDIX A: RELATION BETWEEN BURKARDT AND SOPER DENSITIES

The off-forward parton distribution appropriate for a spin-zero meson in the valence approximation is defined by

$$H(x,\zeta,t) = \int \frac{dy^-}{8\pi} e^{ixP^+y^-/2}\langle P'|\bar{\psi}(0)\gamma^+\psi(y^-)|P\rangle_{y^+=0}$$
$$= \int_0^1 dz\,\delta(x-z)\theta(z-\zeta) \times \int d^2k_\perp \psi^*\left(\frac{z-\zeta}{1-\zeta}, k_\perp - \frac{1-z}{1-\zeta}\Delta_\perp\right)\psi(z,k_\perp). \tag{A1}$$

For skewness $\zeta = 0$,

$$H(x,\zeta=0,t) = H(x,\Delta_\perp) = \int d^2k_\perp \psi^*(x,k_\perp - (1-x)\Delta_\perp)\psi(x,k_\perp) = \int \frac{d^2b_\perp}{(2\pi)^2} e^{-i(1-x)b_\perp\cdot\Delta_\perp}\phi^*(x,b_\perp)\phi(x,b_\perp), \tag{A2}$$

where the FT of the wave function is defined as

$$\psi(x,k_\perp) = \int \frac{d^2b_\perp}{(2\pi)^2} e^{-ib_\perp\cdot k_\perp}\phi(x,b_\perp). \tag{A3}$$

The transverse Fourier transform of the zero skewness off-forward parton distribution H [6] yields the impact parameter density function

$$\int \frac{d^2\Delta_\perp}{(2\pi)^2} e^{i\eta_\perp\cdot\Delta_\perp} H(x,\Delta_\perp) = \int d^2b_\perp \delta^2[(1-x)b_\perp - \eta_\perp] \times \phi^*(x,b_\perp)\phi(x,b_\perp) = \frac{\rho(x,\frac{\eta_\perp}{1-x})}{1-x}, \tag{A4}$$

where $\rho(x,b_\perp)$ is the Soper density defined in Eq. (5) of Ref. [8]. We thus find that the density obtained by Burkardt is the same as the Soper density.

APPENDIX B: REGULATORS

Let us consider the real part of the DVCS amplitude for electrons in one-loop QED given by

$$\mathrm{Re}\ M(\zeta,\Delta_\perp) = -e^2\int_0^\zeta dx F^{31}(x,\zeta,\Delta_\perp)\left[\frac{1}{x}+\frac{1}{x-\zeta}\right] - e^2\int_\zeta^1 dx F^{22}(x,\zeta,\Delta_\perp)\left[\frac{1}{x}+\frac{1}{x-\zeta}\right] \tag{B1}$$

which results after performing the transverse momentum integration. As described in the text, we use an ultraviolet cutoff Λ on the transverse momentum.

The integrands for various DVCS amplitudes may exhibit singular behavior when x is near the end points. We also have a potential singularity when $x \to \zeta$, which can be regulated by using the principal value prescription. In the numerical work we implement the principal value prescription by employing suitable regulators and ensuring regulator independence in the limit where the regulator vanishes. We also note that we eventually integrate over ζ which ranges between $\zeta_{\min}$, which is close to zero, and $\zeta_{\max}$, which is determined by $-t$ and approaches 1 in the limit $-t \to \infty$.

The light-cone momentum fractions must remain positive. Let $\zeta_{\min} = \zeta + \epsilon/2$ for the second integral. Since $\zeta_{\max} = 1-\epsilon$, to make sure that x remains greater than ζ in the second integral, we choose $x_{\max}$ in the second integral to be $1-\epsilon/2$. Thus the regulated integral is

$$\mathrm{Re}\,M(\zeta,\Delta_\perp) = -e^2\int_{\epsilon/2}^{\zeta-\epsilon/2} dx F^{31}(x,\zeta,\Delta_\perp)\left[\frac{1}{x}+\frac{1}{x-\zeta}\right] - e^2\int_{\zeta+\epsilon/2}^{1-\epsilon/2} dx F^{22}(x,\zeta,\Delta_\perp)\left[\frac{1}{x}+\frac{1}{x-\zeta}\right]. \tag{B2}$$

It is important to note that, when ζ is small, a significant contribution to the integral comes from the second term that involves F^{22} and, when ζ is large, a significant contribution to the integral comes from F^{31}. For the helicity-flip case, both F^{22} and F^{31} vanish as $x \to 0$. For the helicity-nonflip amplitude, F^{31} vanishes as $x \to 0$, but F^{22} is finite as $x \to 0$. Thus the only potential problem at small x occurs in Eq. (B2) for the *second term* involving F^{22} when ζ is small, and we obtain a logarithmic divergence due to this problem. This is directly related to the nonvanishing of the electron wave function as $x \to 0$. For helicity nonflip, the function F^{22} also diverges as $x \to 1$. In this region, the DVCS amplitude also receives contributions from the single-particle sector of the Fock space which we do not take into account in the present calculation. If one uses an invariant mass cutoff, the divergences at

$x = 0$ and $x = 1$ would have been regulated by nonzero electron and photon masses, respectively. These regulators are not mandatory in our present calculations, and we have employed the simpler regulators as described above.

APPENDIX C: AN ILLUSTRATIVE MODEL

Let us start from the expression for the Fourier transform,

$$A(\sigma) = \frac{1}{2\pi}\int d\zeta e^{i\sigma\zeta} M(\zeta). \tag{C1}$$

The function $A(\sigma)$ is in coordinate space and the function $M(\zeta)$ is in momentum space.

Let us approximate M by the following function:

$$\begin{aligned} M(\zeta) &= M_0 \quad \text{for } 0 < \zeta < \zeta_{\max} \\ &= 0 \quad \text{for } \zeta > \zeta_{\max}. \end{aligned} \tag{C2}$$

One can use this step function to approximate a DVCS amplitude in which the dependence of the DVCS amplitude in ζ is almost flat; in such a case we can take $M_0 = [M(\zeta = 0) + M(\zeta = \zeta_{\max}]/2$.

We have

$$\begin{aligned} A(\sigma) &= \frac{M_0}{2\pi}\int_0^{\zeta_{\max}} d\zeta e^{i\sigma\zeta} \\ &= \frac{M_0\zeta_{\max}}{2\pi}\frac{\sin(\sigma\zeta_{\max}/2)}{\sigma\zeta_{\max}/2} e^{i\sigma\zeta_{\max}/2}. \end{aligned} \tag{C3}$$

In this case, note that the cosine and sine transforms are completely in phase, and the phase of the Fourier transform does not contain any extra information. The amplitude (i.e., the Fourier spectrum) is given by

$$|A(\sigma)| = \frac{M_0\zeta_{\max}}{2\pi}\frac{|\sin(\sigma\zeta_{\max}/2)|}{\sigma\zeta_{\max}/2}. \tag{C4}$$

The magnitude of the peak of the diffraction pattern

$$A(\sigma)_{\max} = \frac{M_0\zeta_{\max}}{2\pi} \tag{C5}$$

and the first diffraction minimum occurs at

$$\sigma_1 = \frac{2\pi}{\zeta_{\max}}. \tag{C6}$$

In the case of the DVCS amplitude whose functional dependence on ζ is very weak, we can further predict the position of the minima as follows. The extension of the function $\zeta_{\max}$ is given by

$$\zeta_{\max} = \frac{-t}{2M^2}\left(\sqrt{1 + \frac{4M^2}{-t}} - 1\right). \tag{C7}$$

Thus we find a precise relation between the minima of the diffraction pattern and $-t$. Since σ_1 is inversely proportional to $\zeta_{\max}$, which in turn increases with $-t$, the inward movement of the first minimum with increasing $-t$ is readily explained. On the other hand, the peak height is a product of M_0 and $\zeta_{\max}$. The amplitude M_0 decreases monotonically with increasing $-t$. On the other hand, $\zeta_{\max}$ increases with increasing $-t$. Thus the peak height has nonmonotonic behavior with respect to $-t$.

TABLE III. Simplified approximation for the real part of the helicity-nonflip DVCS amplitude shown in Figs. 14(a) and 14(b). The energy quantities are given in MeV and lengths are in MeV^{-1}.

$\sqrt{-t}$	$\zeta_{\max}$	M_0	Peak $(\frac{M_0\zeta_{\max}}{2\pi})$	1st minimum $(\sigma_1 = \frac{2\pi}{\zeta_{\max}})$
100	0.48	0.04	3×10^{-3}	13.09
316	0.84	0.03	4×10^{-3}	7.48
707	0.96	0.0175	2.7×10^{-3}	6.54

In Table III we compare the numbers with the case of the real part of the helicity-nonflip amplitude presented in Figs. 14(a) and 14(b). Similarly, one can also obtain estimates for the helicity-flip amplitudes.

The essential ingredients for the diffraction pattern in the Fourier spectrum are two characteristics of the DVCS amplitudes in the variable ζ:

(i) A step (i.e., a sharp rise) and

(ii) a plateau.

These are the essential characteristics of a function which is almost a constant that seems to be shared by the DVCS amplitudes which produce a diffraction pattern in the FS. The imaginary part of the helicity-flip DVCS amplitude for the electron state [Fig. 5(a)] lacks these properties and we do not observe any diffraction pattern in the corresponding Fourier spectrum [Fig. 7(a)].

It is interesting to note that the simple model we have discussed in this appendix appears in antenna theory [38]. In the case of an aperture for which a uniform electric field is maintained over a finite distance, outside of which the field is zero, the angular spectrum which is the Fourier spectrum of the aperture field distribution exhibits the diffraction pattern discussed in this appendix.

APPENDIX D: DVCS AMPLITUDE IN THREE DIMENSIONS

The significance of the amplitude in the boost-invariant σ space can also be explained in the following way. The Dirac and Pauli form factors $F_1(t)$ and $F_2(t)$, respectively, can be expressed in terms of the helicity-nonflip part of the off-forward matrix element.

Let us consider the dressed electron in the frame $\zeta = 0$. The form factor can be written as [8]

$$F(t) = \int_0^1 dx \int d^2b^\perp e^{-i\Delta^\perp\cdot b^\perp} |\tilde{\psi}_2(x, b^\perp)|^2. \tag{D1}$$

The LFWFs in the mixed representation x, $b^\perp$ are given by

Eq. (1) of [24]. Note that the LFWFs are zero outside the region $0 < x < 1$. We denote

$$\Psi_2(x, b^\perp) = \tilde{\psi}_2(x, b^\perp)\theta(x)\theta(1-x),$$
$$\Psi_3(x_1, x_2, b_1^\perp, b_2^\perp) = \tilde{\psi}_3(x_1, x_2, b_1^\perp, b_2^\perp)\theta(x_1)\theta(x_2) \times \theta(1-x_1)\theta(1-x_2) \quad \text{(D2)}$$

for the two-particle LFWF, and similarly Ψ_2 for the three-particle wave function. We take FT of the LFWFs Ψ with respect to x, and define

$$\Phi_n(\sigma_i, b_i^\perp) = \left\{\Pi_{i=1}^{n-1}\int_{-\infty}^{+\infty} d\sigma_i e^{-i\sigma_i x_i}\right\}\Psi_n(x_i, b_i^\perp), \quad \text{(D3)}$$

where σ_i are the boost-invariant longitudinal distances on the light cone, conjugate to $x_i = k_i^+/P^+$. There are $n-1$ independent σ_i as well as $b_i^\perp$. In terms of these, we can write

$$F(t) = \int dx \int d^2b^\perp e^{-i\Delta^\perp\cdot b^\perp}\int d\sigma_1\int d\sigma_2 e^{i\sigma_1 x}e^{-i\sigma_2 x}\Phi_2^*(\sigma_1, b^\perp)\Phi_2(\sigma_2, b^\perp) = 2\pi\int d^2b^\perp e^{-i\Delta^\perp\cdot b^\perp}\int d\sigma|\Phi_2(\sigma, b^\perp)|^2. \quad \text{(D4)}$$

Note that, as Φ_n are the FT of the wave functions Ψ_n rather than $\tilde{\psi}_n$, it is mathematically correct to take the x integrals from $-\infty$ to $+\infty$. When ζ is nonzero, the form factor receives contributions from $2-2$ and $3-1$ components of the GPDs H and E. They can be obtained from

$$\int dx[F_{++}^{22}(x,\zeta,t)\theta(x-\zeta) + F_{++}^{31}(x,\zeta,t)\theta(\zeta-x)] = \sqrt{1-\zeta}F_1(t) - \frac{\zeta^2}{4\sqrt{1-\zeta}}F_2(t)$$
$$\approx \int_0^1 dx\int d^2b^\perp e^{-i\Delta^\perp\cdot b^\perp}\Big[\sqrt{1-\zeta}\tilde{\psi}_3^\uparrow(x, 1-\zeta, \zeta-x, -b^\perp)\theta(\zeta-x) + \tilde{\psi}_2^{*\uparrow}\Big(x', \frac{b^\perp}{1-x'}\Big)\tilde{\psi}_2^\uparrow\Big(x, \frac{b^\perp}{1-x'}\Big)\frac{(1-\zeta)^2}{(1-x)^2}\theta(x-\zeta)\Big], \quad \text{(D5)}$$

$$\int_0^1 dx[F_{+-}^{22}(x,\zeta,t)\theta(x-\zeta) + F_{+-}^{31}(x,\zeta,t)\theta(\zeta-x)] = \frac{1}{\sqrt{1-\zeta}}\frac{(\Delta^1 - i\Delta^2)(1-\zeta/2)}{2M}F_2(t)$$
$$\approx \int_0^1 dx\int d^2b^\perp e^{-i\Delta^\perp\cdot b^\perp}\Big[\sqrt{1-\zeta}\tilde{\psi}_3^\downarrow(x, 1-\zeta, \zeta-x, -b^\perp)\theta(\zeta-x) + \tilde{\psi}_2^{*\uparrow}\Big(x', \frac{b^\perp}{1-x'}\Big)\tilde{\psi}_2^\downarrow\Big(x, \frac{b^\perp}{1-x'}\Big)\frac{(1-\zeta)^2}{(1-x)^2}\theta(x-\zeta)\Big]. \quad \text{(D6)}$$

$x' = \frac{x-\zeta}{1-\zeta}$. Here we have suppressed the explicit helicity indices and used

$$F_1(t) = \int_0^1 \frac{H(x,\zeta,t)}{1-\frac{\zeta}{2}}, \qquad F_2(t) = \int_0^1 \frac{E(x,\zeta,t)}{1-\frac{\zeta}{2}}. \quad \text{(D7)}$$

The form factors $F_1(t)$ and $F_2(t)$ can be obtained in terms of overlaps of LFWFs in the mixed representation $\tilde{\psi}_n$ from Eqs. (D5) and (D6). Note that, as the arguments of the wave functions are $\frac{b^\perp}{1-x'}$, these equations cannot be expressed as an overlap of the FT wave functions $\Phi_n(\sigma_i, b_i^\perp)$ in position space.

However, in the mixed representation, one can write

$$F_1(t) = \int d^2b^\perp e^{i\Delta^\perp\cdot b^\perp}\Big[\int_0^\zeta dx R_{31}(x,\zeta,b^\perp) + \int_\zeta^1 dx R_{22}(x,\zeta,b^\perp)\Big] = \int_0^1 dx\int d^2b^\perp e^{i\Delta^\perp\cdot b^\perp}R(x,\zeta,b^\perp)$$
$$= \int_0^1 dx\int d^2b'^\perp e^{i\Delta'^\perp\cdot b'^\perp}\rho(x, b'^\perp); \quad \text{(D8)}$$

$$F_2(t) = \int d^2b^\perp e^{i\Delta^\perp\cdot b^\perp}\Big[\int_0^\zeta dx\tilde{R}_{31}(x,\zeta,b^\perp) + \int_\zeta^1 dx\tilde{R}_{22}(x,\zeta,b^\perp)\Big] = \int_0^1 dx\int d^2b^\perp e^{i\Delta^\perp\cdot b^\perp}\tilde{R}(x,\zeta,b^\perp)$$
$$= \int_0^1 dx\int d^2b'^\perp e^{i\Delta'^\perp\cdot b'^\perp}\tilde{\rho}(x, b'^\perp). \quad \text{(D9)}$$

$R(x,\zeta,b^\perp)$ and $\tilde{R}(x,\zeta,b^\perp)$ can be obtained in terms of off-diagonal overlaps of LFWFs $\tilde{\psi}_n(x_i, b_i^\perp)$ which in turn can be

obtained from the above equations. $\rho(x, b'^{\perp})$ and $\tilde{\rho}(x, b'^{\perp})$ are Soper's distributions in the frame $\zeta = 0$. It can be shown that

$$\tilde{\rho}(x, b^{\perp}) = -2iM \frac{\partial}{\partial b} \frac{(b^1 + ib^2)}{b} \rho(x, b^{\perp}). \tag{D10}$$

Equations (D8) and (D9) show the relation between the generalized correlation functions R and $\tilde{R}$ with Soper's distribution due to covariance of the form factor. However, the functions R and $\tilde{R}$ do not have a probability interpretation, unlike Soper's distribution.

In the imaginary part of the DVCS amplitude, we have the GPDs integrated with a delta function,

$$\mathrm{Im}[M^{++}] = N \int_0^1 dx \left[\delta(x - \zeta) \frac{\sqrt{1-\zeta}}{1 - \frac{\zeta}{2}} H_{(2\to 2)}(x, \zeta, t) - \frac{\zeta^2}{4(1 - \frac{\zeta}{2})\sqrt{1-\zeta}} E_{(2\to 2)}(x, \zeta, t) \delta(\zeta - x) \right]. \tag{D11}$$

In terms of the correlation functions defined above, this can be written as

$$\begin{aligned} \mathrm{Im}[M^{++}] &= N \int d^2 b^{\perp} e^{i\Delta^{\perp}\cdot b^{\perp}} \int_0^1 dx \Big\{ \sqrt{1-\zeta} [\theta(\zeta - x) R_{31}(x, \zeta, b^{\perp}) + \theta(x - \zeta) R_{22}(x, \zeta, b^{\perp})] \delta(x - \zeta) \\ &\quad - \frac{\zeta^2}{4\sqrt{1-\zeta}} [\theta(\zeta - x) \tilde{R}_{31}(x, \zeta, b^{\perp}) + \theta(x - \zeta) \tilde{R}_{22}(x, \zeta, b^{\perp})] \delta(x - \zeta) \Big\} \\ &= \int d^2 b^{\perp} e^{i\Delta^{\perp}\cdot b^{\perp}} \int_0^1 dx \Big\{ \sqrt{1-\zeta} R(x, \zeta, b^{\perp}) \delta(x - \zeta) - \frac{\zeta^2}{4\sqrt{1-\zeta}} \tilde{R}(x, \zeta, b^{\perp}) \delta(x - \zeta) \Big\}. \end{aligned} \tag{D12}$$

N is the normalization constant. Integrating over x we obtain

$$\mathrm{Im}[M^{++}] = N \int d^2 b^{\perp} e^{i\Delta^{\perp}\cdot b^{\perp}} \left\{ \sqrt{1-\zeta} R(x = \zeta, b^{\perp}) - \frac{\zeta^2}{4\sqrt{1-\zeta}} \tilde{R}(x = \zeta, b^{\perp}) \right\}. \tag{D13}$$

Thus, the FT of the imaginary part of the DVCS amplitude with respect to $\Delta^{\perp}$ gives both $R(x, \zeta, b_{\perp})$ and $\tilde{R}(x, \zeta, b_{\perp})$, where x of the struck parton is now fixed at $x = \zeta$. These, in turn, are related to Soper's distributions $\rho(x, b^{\perp})$ through Eqs. (D8) and (D9). This is a mixed coordinate and momentum space representation. The above relation can be generalized to a hadron in a model independent way. Introducing the complete 3D spatial amplitude $\bar{\rho}(\sigma, b^{\perp})$ at fixed light-front time τ, we can write

$$\mathrm{Im}[M^{++}] = N \int d\sigma e^{-i\sigma\zeta} \int d^2 b^{\perp} e^{-i\Delta^{\perp}\cdot b^{\perp}} \bar{\rho}(\sigma, b^{\perp}). \tag{D14}$$

Here σ is conjugate to ζ. Note that, as we are at fixed τ rather than at fixed time, there is no conceptual problem due to Lorentz boosts.

The physics of the real part of the DVCS amplitude is more involved. However, it is related to the imaginary part by a dispersion relation in x. The real part can be expressed in terms of the densities ρ and $\tilde{\rho}$ as well; however, it contains a principal value (PV) integral over x. We can call the result of the PV integral $\gamma(\zeta, b^{\perp})$. Again, after taking a FT in ζ, we obtain the amplitude in full 3D coordinate space.

[1] A. V. Radyushkin, Phys. Rev. D **56**, 5524 (1997); X. Ji and J. Osborne, Phys. Rev. D **58**, 094018 (1998); J. C. Collins and A. Freund, Phys. Rev. D **59**, 074009 (1999).

[2] S. J. Brodsky, F. E. Close, and J. F. Gunion, Phys. Rev. D **5**, 1384 (1972); **6**, 177 (1972); **8**, 3678 (1973).

[3] P. Kroll, M. Schurmann, and P. A. Guichon, Nucl. Phys. **A598**, 435 (1996); M. Diehl, T. Gousset, B. Pire, and J. P. Ralston, Phys. Lett. B **411**, 193 (1997); A. V. Belitsky, D. Muller, L. Niedermeier, and A. Schafer, Phys. Lett. B **474**, 163 (2000).

[4] S. J. Brodsky, M. Diehl, and D. S. Hwang, Nucl. Phys. **B596**, 99 (2001).

[5] M. Diehl, T. Feldmann, R. Jacob, and P. Kroll, Nucl. Phys. **B596**, 33 (2001); **B605**, 647(E) (2001).

[6] M. Burkardt, Int. J. Mod. Phys. A **18**, 173 (2003).

[7] M. Burkardt, Phys. Rev. D **62**, 071503 (2000); **66**,

119903(E) (2002); J. P. Ralston and B. Pire, Phys. Rev. D **66**, 111501 (2002).
[8] D. E. Soper, Phys. Rev. D **15**, 1141 (1977).
[9] P. A. M. Dirac, Rev. Mod. Phys. **21**, 392 (1949).
[10] D. Chakrabarti, A. Harindranath, and J. P. Vary, Phys. Rev. D **71**, 125012 (2005); D. Chakrabarti, A. Harindranath, L. Martinovic, G. B. Pivovarov, and J. P. Vary, Phys. Lett. B **617**, 92 (2005); D. Chakrabarti, A. Harindranath, L. Martinovic, and J. P. Vary, Phys. Lett. B **582**, 196 (2004).
[11] X. Ji, Phys. Rev. Lett. **91**, 062001 (2003); A. V. Belitsky, X. Ji, and F. Yuan, Phys. Rev. D **69**, 074014 (2004).
[12] S. J. Brodsky, D. Chakrabarti, A. Harindranath, A. Mukherjee, and J. P. Vary, Phys. Lett. B **641**, 440 (2006).
[13] S. J. Brodsky and S. D. Drell, Phys. Rev. D **22**, 2236 (1980).
[14] S. J. Brodsky, H. C. Pauli, and S. Pinsky, Phys. Rep. **301**, 299 (1998).
[15] S. J. Brodsky, D. S. Hwang, B.-Q. Ma, and I. Schmidt, Nucl. Phys. **B593**, 311 (2001).
[16] D. Chakrabarti and A. Mukherjee, Phys. Rev. D **71**, 014038 (2005).
[17] D. Chakrabarti and A. Mukherjee, Phys. Rev. D **72**, 034013 (2005).
[18] J. F. Donoghue, B. R. Holstein, B. Garbrecht, and T. Konstandin, Phys. Lett. B **529**, 132 (2002).
[19] A. Harindranath and R. Kundu, Phys. Rev. D **59**, 116013 (1999).
[20] A. Harindranath, R. Kundu, A. Mukherjee, and J. P. Vary, Phys. Rev. D **58**, 114022 (1998); A. Mukherjee and D. Chakrabarti, Phys. Lett. B **506**, 283 (2001); A. Harindranath, A. Mukherjee, and R. Ratabole, Phys. Lett. B **476**, 471 (2000); Phys. Rev. D **63**, 045006 (2001); A. Harindranath, R. Kundu, and W. M. Zhang, Phys. Rev. D 59, 094013 (2001).
[21] A. Mukherjee and M. Vanderhaeghen, Phys. Rev. D **67**, 085020 (2003); Phys. Lett. B **542**, 245 (2002).
[22] A. Mukherjee, I. V. Musatov, H. C. Pauli, and A. V. Radyushkin, Phys. Rev. D **67**, 073014 (2003); S. J. Brodsky and F. J. Llanes-Estrada, Eur. Phys. J. C **46**, 751 (2006).
[23] K. Hornbostel, S. J. Brodsky, and H. C. Pauli, Phys. Rev. D **41**, 3814 (1990).
[24] S. J. Brodsky and G. F. de Teramond, Phys. Rev. Lett. **96**, 201601 (2006).
[25] S. J. Brodsky, P. Hoyer, N. Marchal, S. Peigne, and F. Sannino, Phys. Rev. D **65**, 114025 (2002).
[26] S. J. Brodsky, D. S. Hwang, and I. Schmidt, Phys. Lett. B **530**, 99 (2002).
[27] P. Hoyer, hep-ph/0608295.
[28] W. M. Zhang and A. Harindranath, Phys. Rev. D **48**, 4881 (1993).
[29] A. V. Oppenheim and J. S. Lim, Proc. IEEE **69**, No. 5, 529 (1981).
[30] M. B. Einhorn, Phys. Rev. D **14**, 3451 (1976).
[31] F. Antonuccio, S. J. Brodsky, and S. Dalley, Phys. Lett. B **412**, 104 (1997).
[32] A. Airapetian *et al.* (HERMES Collaboration), Phys. Rev. Lett. **87**, 182001 (2001); S. Stepanyan *et al.* (CLAS Collaboration), Phys. Rev. Lett. **87**, 182002 (2001).
[33] C. R. Ji, Y. Mishchenko, and A. Radyushkin, Phys. Rev. D **73**, 114013 (2006).
[34] E. C. G. Sudarshan, R. Simon, and N. Mukunda, Phys. Rev. A **28**, 2921 (1983); Report No. DOE-ER-03992-503.
[35] N. Mukunda, R. Simon, and E. C. G. Sudarshan, Phys. Rev. A **28**, 2933 (1983); Report No. DOE-ER-03992-504.
[36] R. J. Glauber, in *High-Energy Collision Theory*, Lectures in Theoretical Physics, edited by W. Brittain and L. G. Dunham (Interscience, New York, 1959), Vol. 1, p. 315.
[37] E. Kujawski and J. P. Vary, Phys. Rev. C **12**, 1271 (1975).
[38] R. N. Bracewell, *The Fourier Transform and its Applications* (Tata McGraw-Hill Publishing Company Limited, New Delhi, 2003).